JGR Solid Earth

RESEARCH ARTICLE
10.1029/2019JB019225

The Norwegian-Greenland Sea, the Laschamps, and the Mono Lake Excursions Recorded in a Black Sea Sedimentary Sequence Spanning From 68.9 to 14.5 ka

Jiabo Liu[1,2], **Norbert R. Nowaczyk**[1], **Sanja Panovska**[3], **Monika Korte**[3], **and Helge W. Arz**[4]

[1]GFZ German Research Centre for Geosciences, Section 4.3, Helmholtz Centre Potsdam, Potsdam, Germany, [2]Now at Department of Ocean Science and Engineering, Southern University of Science and Technology, Shenzhen, China, [3]GFZ German Research Centre for Geosciences, Section 2.3, Helmholtz Centre Potsdam, Potsdam, Germany, [4]Leibniz Institute for Baltic Sea Research Warnemünde, Rostock, Germany

Key Points:
- Reconstructed paleosecular variation record between 68.9 and 14.5 ka from Black Sea sediments
- Increasing axial dipole component with reversed polarity during the midpoint of the Laschamps excursion
- Comparable levels of dipole and nondipole contributions during the Mono Lake excursion

Supporting Information:
- Supporting Information S1

Correspondence to:
J. Liu and N. R. Nowaczyk,
liujb@sustch.edu.cn;
norbert.nowaczyk@gfz-potsdam.de

Citation:
Liu, J., Nowaczyk, N. R., Panovska, S., Korte, M., & Arz, H. W. (2020). The Norwegian-Greenland Sea, the Laschamps, and the Mono Lake excursions recorded in a Black Sea sedimentary sequence spanning from 68.9 to 14.5 ka. *Journal of Geophysical Research: Solid Earth*, *125*, e2019JB019225. https://doi.org/10.1029/2019JB019225

Received 17 DEC 2019
Accepted 4 AUG 2020
Accepted article online 6 AUG 2020

Abstract A full-vector paleomagnetic record, comprising directional data and relative paleointensity (rPI), was derived from 16 sediment cores recovered from the southeastern Black Sea. The obtained data were used to create a stack covering the time window between 68.9 and 14.5 ka. Age models are based on radiocarbon dating and correlations of warming/cooling cycles monitored by high-resolution X-ray fluorescence (XRF) elementary ratios and by ice-rafted debris (IRD) in Black Sea sediments to the sequence of "Dansgaard-Oeschger" (D-O) events defined from the Greenland ice core oxygen isotope stratigraphy. The reconstructed prominent lows in paleointensity at about 64.5, 41.2, and 34.5 ka are coeval with the Norwegian-Greenland Sea, the Laschamps, and the Mono Lake excursions, respectively. For a further analysis, the stacked Black Sea paleomagnetic record was converted into one component being parallel to the direction expected from a geocentric axial dipole (GAD) and two components perpendicular to it (EW, inclined NS), representing definitely only non-GAD components of the geomagnetic field. Discussions of the field configurations at the Black Sea site are focused on the three excursional events. The Norwegian-Greenland Sea excursion was dominated by a decaying axial dipole and persisting weak nondipole field, with directional variations still within the range of normal secular variations. The Laschamps excursion comprises two full polarity transitions and a short stable interval of reversed polarity in between. The Mono Lake excursion was mostly dominated by a nondipole field, though with a less pronounced weakening of the axial dipole component.

1. Introduction

Paleosecular variation (PSV) records obtained from paleomagnetic archives, such as archeological artifacts, volcanic rocks, and sediments, are an expression of geodynamo processes inside the Earth's liquid outer core (e.g., Merrill & McFadden, 1999). These paleomagnetic time series provide insights into the properties of the Earth's magnetic field, from normal behaviors with a dominating dipolar geometry, over field crises, such as geomagnetic excursions with a distorted field geometry, to the complete reversal of the dominating dipole contribution (e.g., Channell et al., 2020; Laj & Channell, 2015; Roberts, 2008; Valet et al., 2005).

Understanding the origin, amplitude, duration, occurrence frequency, and field behavior of geomagnetic excursions is a forefront research area within solid earth geophysics (Roberts, 2008). During the past few decades, substantial efforts have been made on recovering geomagnetic field history from lava flows and sediments (e.g., Cassata et al., 2008; Lund, Stoner, Channell, et al., 2006). In Marine Isotope Stage 4 (MIS 4, 57–71 ka), evident field intensity lows, coeval with the Norwegian-Greenland Sea excursion at around 65 ka, are commonly observed in sedimentary paleomagnetic records (e.g., Channell et al., 2009; Laj et al., 2004; Lund, Stoner, Channell, et al., 2006). However, shallow to steep negative inclinations of the Norwegian-Greenland Sea excursion are exclusively reported in sediments from the Arctic Ocean (e.g., Bleil & Gard, 1989; Løvlie, 1989; Nowaczyk & Frederichs, 1999; Nowaczyk et al., 2003; Xuan et al., 2012). Wiers et al. (2019) and Xuan et al. (2012) postulate that these anomalous paleomagnetic directions might be biased due to oxidation on the seafloor of the Arctic Ocean. In the west Equatorial Pacific Ocean,

Lund, Schwartz, et al. (2017) also reported anomalous directions that can be associated with the Norwegian-Greenland Sea excursion in Sediment Core MD98-2181, though they argued that the data are not truly excursional. Hence, the Norwegian-Greenland Sea excursion is obviously not yet very well documented and remains fuzzy regarding to its field configuration.

The Laschamps excursion (we use the spelling according to Kornprobst & Lénat, 2019), centered at about 41 ka, is the best studied excursion event (e.g., Bonhommet & Babkine, 1967; Cassata et al., 2008; Channell et al., 2020; Gillot et al., 1979; Ingham et al., 2017; Laj & Channell, 2015; Ménabréaz et al., 2011; Plenier et al., 2007). Virtual geomagnetic pole (VGP) paths derived from seven sedimentary records (separated by 178° in longitude and 113° in latitude) exhibit a coherent clockwise loop during the Laschamps excursion (Laj et al., 2006). Therefore, they suggested that this consistency of VGP paths indicates a relatively simple, possibly dominating dipolar, excursional field geometry. Nevertheless, this scenario has been questioned by VGPs of the Laschamps obtained from lava flows that do not coincide with the longitudinal loops seen in the sedimentary records of Laj et al. (2006) and are only compatible with a dominant nondipolar field geometry (e.g., Cassata et al., 2008; Ingham et al., 2017; Plenier et al., 2007).

The Mono Lake excursion (Denham & Cox, 1971; Liddicoat & Coe, 1979; Lund et al., 1988) at about 35 ka has been evidenced as an excursion distinct from the Laschamps excursion (e.g., Cassata et al., 2008; Channell, 2006; Kissel et al., 2011). The smaller magnitude of directional variations during the Mono Lake excursion combined with its shorter duration makes it even more difficult to detect in sediment cores when compared with the Laschamps excursion (Cassidy & Hill, 2009). During the Mono Lake excursion, intensity lows coeval with anomalous directions have been globally reported (e.g., Cassata et al., 2008; Kissel et al., 2011; Lund et al., 1988; Negrini et al., 2014). But available VGPs from different sites or even very close sites (e.g., Summer Lake, Negrini et al., 2014; Mono Lake, Lund et al., 1988) exhibit distinct VGP paths (see Figure 8 in Liu et al., 2019). The currently available VGP paths with apparent discrepancies are probably not yet adequate to reach a satisfying description of the field behavior during the Mono Lake excursion (Kissel et al., 2011; Liu et al., 2019). Nevertheless, Negrini et al. (2014) suggested that the VGPs during the Mono Lake excursion cluster at certain locations which coincide with nonaxial dipole features found in the Holocene geomagnetic field.

In general, geomagnetic excursions remain one of the less well-understood aspects in the spectrum of geomagnetic field behaviors. Simulations of excursions indicate that the presence of antipodal directions, which are observed in most detailed paleomagnetic records of "excursions," requires a small recovery of the field's dipole contribution with the opposite polarity (Valet & Plenier, 2008). In all cases the transitional directions (which refer to the transit between the two polarities) are constrained by variations of the nondipole field (Valet et al., 2008). Based on the reconstruction of geomagnetic field evolution during the Laschamps excursion, Leonhardt et al. (2009) argued that the reconstructed dynamic nondipolar components lead to considerable deviations among predicted records at different locations, though the dipolar field at the Earth's surface was in dominance. By imposing changes on the axial dipole component of the Holocene Geomagnetic Field Model CALS10k.2, Brown and Korte (2016) found that global directional reversals only appear when the axial dipole was reversed in polarity and gained at least 20% of its preexcursional strength in the opposite direction at the excursion midpoint. Based on a geomagnetic field model, covering both the Laschamps and the Mono Lake excursions, Brown et al. (2018) suggested that the geomagnetic field has two possible mean states, one is broadly stable when the axial dipole is dominant at the core-mantle boundary (CMB) and one in which the axial dipole strength matches the higher-degree multipoles and when fluctuations in the axial dipole can produce an excursion. This hypothesis was further expanded by Korte et al. (2019), postulating that (at least) three states of the geomagnetic field, mainly due to the axial dipole contribution, can be established. The nonaxial dipole field, however, might remain relatively unchanged during secular variations and excursions (Korte et al., 2019; Wicht & Meduri, 2016). In addition, excursions with distinct field configurations can exhibit various behaviors in time and geomagnetic field morphologies at different sites on Earth. By using statistical analysis of sedimentary paleomagnetic records from different sites, Lund (2018) suggested that directional fluctuations are more significant during low field intensities or excursional intervals.

Thus, paleomagnetic studies from sediments, which ideally permit precise dating and development of good sequential records of both paleomagnetic directional and intensity variations, have significantly improved

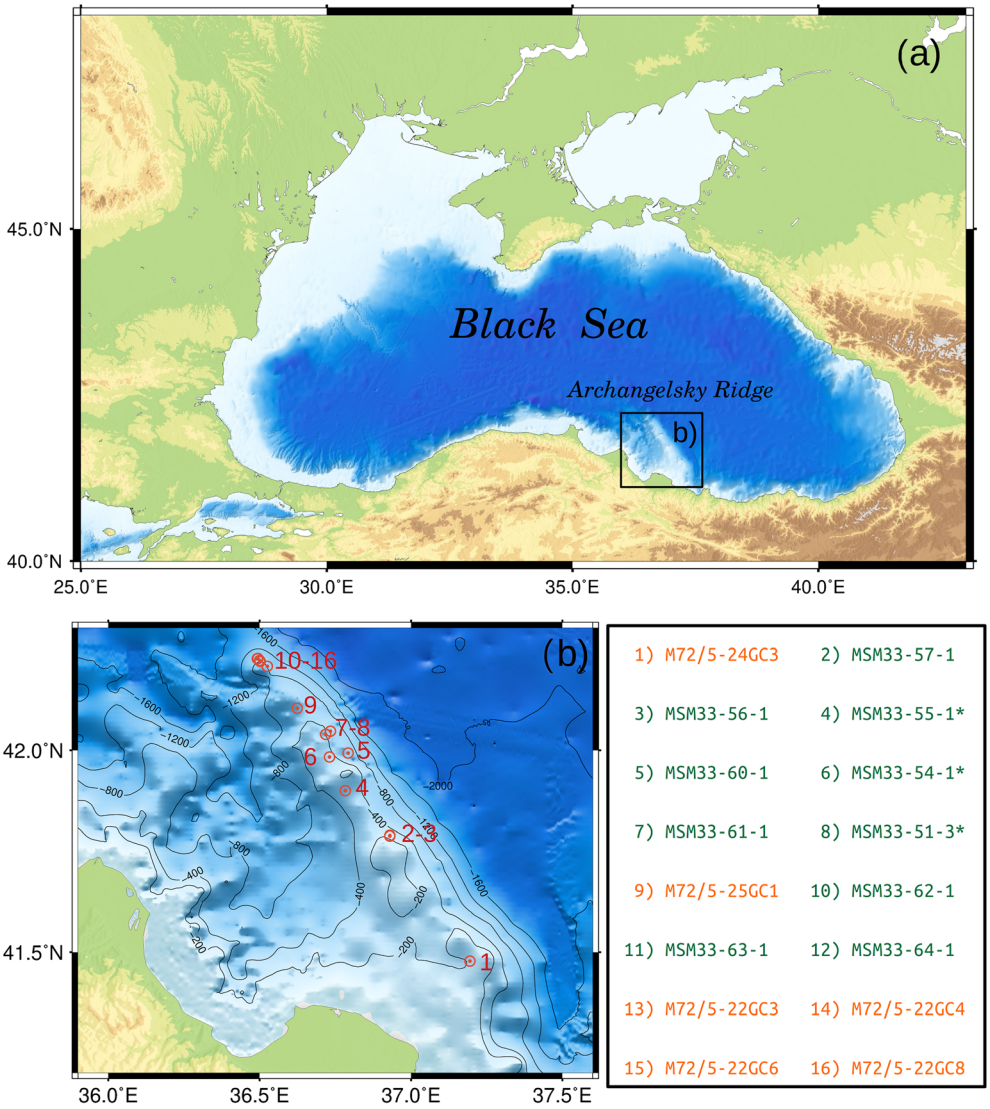

Figure 1. (a) Location of the study area (black rectangle) in the southeastern Black Sea. (b) Investigated sediment cores were recovered along the Archangelsky Ridge during Expeditions M72/5 (2007) and MSM33 (2013). Note that core labels with (without) symbol "*" indicate piston (gravity) cores.

our understandings of the geomagnetic field (e.g., Channell et al., 2020; Laj & Channell, 2015; Laj et al., 2000, 2004; Lund, Stoner, Channell, et al., 2006). In the southeastern Black Sea, six cores were taken from the Archangelsky Ridge by German research vessel *RV METEOR* during Expedition M72/5 in 2007 (Figure 1). As a first result, a high-quality and high-resolution record of the Laschamps excursion (~41 ka) and a high-resolution record of relative paleointensity (rPI) from 68 to 14 ka, based on the six M72/5 cores, could be derived (Nowaczyk et al., 2012, 2013). Ten further cores were taken in the same region by German research vessel *RV Maria S. Merian* during Expedition MSM33 in 2013 (Figure 1). Though supplemented with more data obtained from these new MSM33 cores from the same region, the extended data sets had to be compiled in time intervals with different temporal resolution and with variable data quality (Table 1). This is due to locally and temporarily highly variable sedimentation rates, detected hiatuses, and partly massive contamination by diagenetically precipitated greigite that made parts of the obtained records useless. The greigite-bearing sediments in samples from the Black Sea are generally characterized by ideal single domain (SD) particles and extremely high magnetic susceptibility, mostly due to a locally high greigite concentration. Hence, detailed mineral magnetic analyses were performed

Table 1
Coring Locations, Sampling, and Analysis Statistics for Investigated Cores From RV Meteor Expedition M72/5 (2007) and RV Maria S. Merian Expedition MSM33 (2013)

						Age intervals for stacking inclination, declination, and relative paleointensity				
						14.5–20.0 ka	20.1–39.40 ka	39.44–42.6 ka	42.7–59.0 ka	59.1–68.9 ka
						Stack resolution				
Core number	Site latitude	Site longitude	Water depth (m)	Core length (cm)	Collected samples	50 a[a]	100 a[b]	40 a[c]	100 a[d]	100 a[e]
M72/5-24GC3	41° 28.66′N	37° 11.68′ E	208.0	885	449	#	#			
MSM33-55-1 PC	41° 54.01′N	36° 46.98′ E	362.4	948	403	#	#			#
MSM33-56-1	41° 47.33′N	36° 55.81′ E	373.9	736	302					
MSM33-57-1	41° 47.38′N	36° 55.95′ E	374.0	778	323	#	#			
MSM33-54-3 PC	41° 58.99′N	36° 43.85′ E	382.2	953	413	#	#			#
M72/5-25GC1	42° 06.21′N	36° 37.43′ E	418.0	952	412	#	#			
MSM33-51-3 PC	42° 02.38′N	36° 43.08′ E	428.4	1,027	375	#	#			#
MSM33-61-1	42° 02.85′N	36° 44.02′ E	479.3	746	314	#	#			
MSM33-60-1	41° 58.62′N	36° 47.53′ E	498.8	739	395	#				
MSM33-64-1	42° 12.46′N	36° 31.52′ E	660.5	721	392	#			#	#
MSM33-62-1	42° 13.15′N	36° 30.11′ E	767.3	747	331	#				#
MSM33-63-1	42° 13.27′N	36° 30.00′ E	785.5	704	348	#				#
M72/5-22GC3	42° 13.53′N	36° 29.55′ E	838.0	839	318	#		#	#	
M72/5-22GC4	42° 13.54′N	36° 29.53′ E	842.0	866	393	#		#	#	#
M72/5-22GC6	42° 13.57′N	36° 29.65′ E	843.0	800	343	#		#	#	#
M72/5-22GC8	42° 13.53′N	36° 29.59′ E	847.0	945	372	#		#	#	#

Note. The symbol "#" indicates data availablity for speicific time intervals.
[a]Liu et al. (2018). [b]Liu et al. (2019). [c]Nowaczyk et al. (2012, 2013). [d]This study. [e]Nowaczyk et al. (2018).

on all studied cores that enabled an exclusion of greigite-bearing samples from the paleomagnetic data records (e.g., Liu et al., 2018, 2019; Nowaczyk et al., 2012, 2013, 2018).

Due to the heterogeneous nature of the compiled data sets from the SE Black Sea, publications of the compiled data sets from a total of 16 sediment cores (Figure 1) were split into several studies in the past decade (Table 1). The obtained PSV record for the time interval from 68.9 to 58 ka, about equivalent with MIS 4, with fast directional changes, though not yet being "excursional," associated with low paleointensities at 64.5 ka was reported by Nowaczyk et al. (2018). The PSV record between 58 and 40 ka, with data sets supplemented by MSM33 cores, is presented in this study. The PSV record spanning from 40 to 20 ka, with the Mono Lake excursion documented with excursional directions and low paleointensities at about 34.5 ka, was recently presented by Liu et al. (2019). For the time interval from 20 to 14 ka (about coeval with MIS 2), the high-resolution Black Sea PSV record exhibits only normal variations without clear evidence for the postulated "Hilina Pali" excursion at 18.5 ka (Liu et al., 2018).

In this paper, the complete PSV record compiled from a total of 16 sediment cores from the SE Black Sea is spanning the time interval from 68.9 to 14.5 ka with temporal resolutions ranging from 40 to 100 years. Detailed descriptions of material and methods are given in supporting information Text S1 and Figure S1. The main focus of this paper is the presentation of all paleomagnetic data obtained from the whole collection of cores. Finally, the Black Sea full-vector PSV record will be discussed on the basis of a transformed record, with one component parallel to the direction expected from a geocentric axial dipole (GAD) and two components perpendicular to it, one in EW direction and one in a tilted NS direction, definitely representing only non-GAD components of the geomagnetic field intending to provide some general insights into the geomagnetic field behavior across excursions.

2. Age Models

Age models of M72/5 cores were constrained by 16 accelerator mass spectrometry (AMS) ^{14}C dating (recalibrated using IntCal13 and shown in Figure 2e) in Core M72/5-24GC3 (Nowaczyk et al., 2012) and by identifications of the Campanian Ignimbrite tephra at 39.3 ± 0.11 ka ("Y5," e.g., De Vivo et al., 2001) and the Cape Riva tephra at 21.8 ± 0.4 ka ("Y2," e.g., Fabbro et al., 2013) in Black Sea sediments reported by

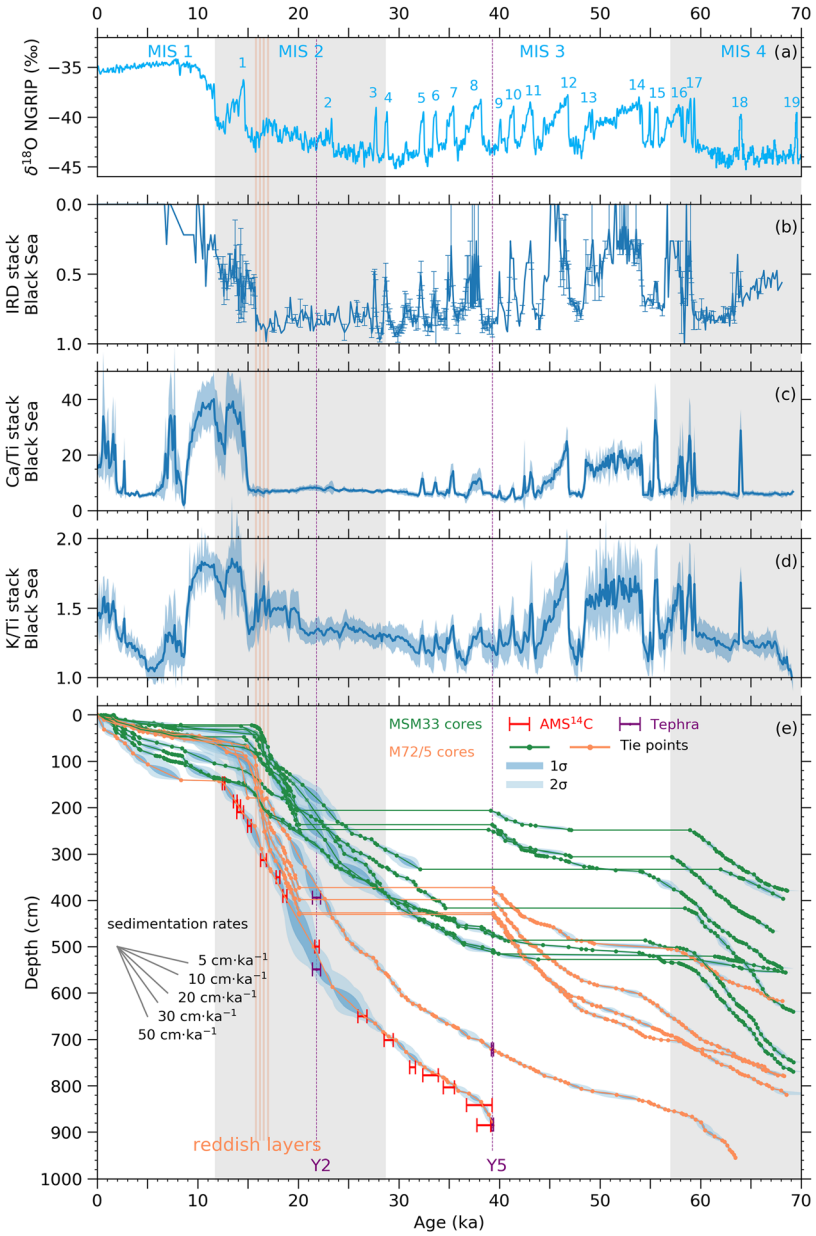

Figure 2. (a) Oxygen isotope record ($\delta^{18}O$) from Greenland ice cores (NGRIP using the GICC05 age model; Svensson et al., 2008) with "Dansgaard-Oeschger" (D-O) warming events (Dansgaard et al., 1993) indicated by numbers 1–19. (b) The stack of Black Sea ice-rafted debris (IRD) counts using 100-year bins was derived from Cores M72/5-22GC8, M72/5-24-GC3, and M72/5-25GC-1 (Nowaczyk et al., 2012). (c) Ca/Ti and (d) K/Ti elementary ratio stacks using 100-year bins were derived from X-ray fluorescence (XRF) scanning of all studied cores (except M72/5-22GC4 and M72/5-22GC6). The stacks of IRD, Ca/Ti, and K/Ti are all plotted with 1σ standard deviation band. IRD counts and Ca/Ti and K/Ti ratios of individual cores correlating to the NGRIP $\delta^{18}O$ record are shown in supporting information Figures S2–S4. (e) Age-depth relationships for the 16 investigated Black Sea cores with highly variable sedimentation rates from 5 to 50 cm ka^{-1} (cf. bundle of lines in the left). AMS ^{14}C ages from Core M72/5-24GC3 (Nowaczyk et al., 2012) are recalibrated using Intcal13 and indicated by red error bars. "Y5" and "Y2" denote the Campanian Ignimbrite tephra at about 39.3 ± 0.11 ka (e.g., De Vivo et al., 2001) and the Cape Riva tephra at about 21.8 ± 0.4 ka (e.g., Fabbro et al., 2013), respectively, identified in Cores M72/5-24GC3 and M72/5-25GC1 (Cullen et al., 2014; Nowaczyk et al., 2012). Tie points were derived from correlations between the NGRIP $\delta^{18}O$ record and IRD counts and Ca/Ti and K/Ti ratios of individual cores in this study (supporting information Figures S2–S4). Reddish layers indicated by four orange bars in the studied cores were correlated to the AMS ^{14}C dated meltwater events (refer to Figure 2 in Liu et al., 2018) reported in the NW Black Sea (Soulet et al., 2013). The 1σ and 2σ age uncertainties of individual cores were estimated by using the software *Undatable* (Lougheed & Obrochta, 2019); for detailed descriptions refer to section 2.

Cullen et al. (2014) and Nowaczyk et al. (2012). The M72/5 cores' age models were further refined by tuning sedimentological parameters, for example, ice-rafted debris (IRD) counts (Figure 2b) and X-ray fluorescence (XRF) logs (mainly Ca/Ti and K/Ti ratios) presented by Nowaczyk et al. (2012), to the oxygen isotope ($\delta^{18}O$) record from North Greenland Ice Core Project (NGRIP) based on the GICC05 age model (Figure 2a; Svensson et al., 2008). IRD counts and Ca/Ti and K/Ti ratios of individual cores correlating to the NGRIP $\delta^{18}O$ record are shown in supporting information Figures S2–S4. Cores M72/5-22GC4 and M72/5-22GC6, which lack XRF scanning results, were synchronized using their high-resolution magnetic susceptibility records, as a common parameter from all cores.

For MSM33 cores, age models were also achieved by correlating XRF elementary ratios (mainly Ca/Ti and K/Ti; see supporting information Figures S3 and S4), as proxies for the "Dansgaard-Oeschger" (D-O) warming events (Dansgaard et al., 1993), to the NGRIP $\delta^{18}O$ record. Ca/Ti and K/Ti stacks, derived from all studied M72/5 and MSM33 cores (except M72/5-22GC4 and M72/5-22GC6), are shown in Figures 2c and 2d, respectively. Between about 30 and 69 ka, the sequence of D-O Events 5–18 is clearly seen in studied Ca/Ti and K/Ti ratio stacks (Figures 2c and 2d), as well as in individual cores (supporting information Figures S3 and S4), if not missing due to hiatuses. Four intervals of K/Ti ratio peaks and low S-ratios identified in M72/5 and MSM33 cores (see Figure 2 in Liu et al., 2018) were correlated to the reddish layers related to meltwater events during the decay of the Fennoscandian ice sheet, with AMS ^{14}C ages from about 17 to 15 ka, described in the western Black Sea (Bahr et al., 2006; Soulet et al., 2013). For sediments younger than 15 ka, Ca/Ti ratio records of investigated cores were correlated to those of Cores GeoB7608-1 (Bahr et al., 2005) and GeoB7622-2 (Lamy et al., 2006) with AMS ^{14}C dating from the western Black Sea (supporting information Figure S3).

Age uncertainties of all studied cores were estimated by using the software *Undatable* (Lougheed & Obrochta, 2019) with setting parameters of xfactor = 0.3 and bootpc = 20. The xfactor scales the widths of Gaussian distribution and the bootpc determines the percentage of age-depth constraints to be bootstrapped in each age-depth model iteration (for details refer to Lougheed & Obrochta, 2019). Although AMS ^{14}C dating between 40 and 25 ka shows a wide range of errors, correlations of X-ray powder diffraction (XRD) counts and Ca/Ti and K/Ti ratios of Core M72/5-24GC3 can provide well-constrained tie points (supporting information Figures S2–S4), as well as the "Y5" tephra layer at 39.3 ± 0.11 ka (Figure 2e). Hence, errors of AMS ^{14}C dating between 40 and 25 ka were not included for estimating age uncertainties in Core M72/5-24GC3. Between about 68.9 and 30 ka, all D-O warming events can be obviously recognized from peaks of Ca/Ti and K/Ti ratios in the studied cores (see supporting information Figures S3 and S4), therefore, yielding very low age uncertainties (Figure 2e). Between about 30 and 18 ka D-O events are not visible in Ca/Ti and K/Ti ratios, but D-O Events 3 and 4, clearly seen in the IRD counts (supporting information Figure S2), and the "Y2" tephra provide further tie points. Thus, age uncertainties are a bit larger compared to other time intervals. From 18 to 14 ka, ages of the studied cores were constrained by the direct AMS ^{14}C dating and by the correlation of reddish meltwater event layers dated by Soulet et al. (2013), resulting in low age uncertainties (Liu et al., 2018).

Obtained age models of investigated sediment cores from Expeditions M72/5 and MSM33 are shown in Figure 2e back until 68.9 ka. Obviously, the end of the last glacial (~14 ka) leads to a dramatic decrease in sedimentation rates from about 50 cm ka^{-1} in MIS 2 down to 5 to 10 cm ka^{-1} in MIS 1. MIS 3 is mostly characterized by sedimentation rates ranging from 20 to 30 cm ka^{-1}, with lowest values in early MIS 3 characterized by generally higher temperatures and longer warming phases (D-O Events 12 to 17), while glacial conditions in the preceding MIS 4 led to higher sedimentation rates.

In many of the studied cores several hiatuses were detected. These gaps in the sedimentary sequences at the slope of the Archangelsky Ridge (Figure 1) are interpreted as the effect of slumping down of sediment packages mobilized by the tectonic (earthquake) activity in this region. The most significant hiatus, detected in all cores, is between about 69 ka (early MIS 4) and 115–120 ka (mid-MIS 5e/Eemian, Wegwerth et al., 2014, 2019). The Eemian in Black Sea sediments is, like the Holocene, built up by soft organic-rich sapropelitic sediments, whereas the glacial sediments are built up by fairly stiff clays (Wegwerth et al., 2014). Presumably, this large difference in shear resistance of the sediments deposited since MIS 5d until early MIS 4 led to the slumping down of these stiff deposits over large areas of the Archangelsky Ridge triggered by a strong earthquake at around 69 ka. The lower (older) sections in all studied cores, except Cores M72/5-

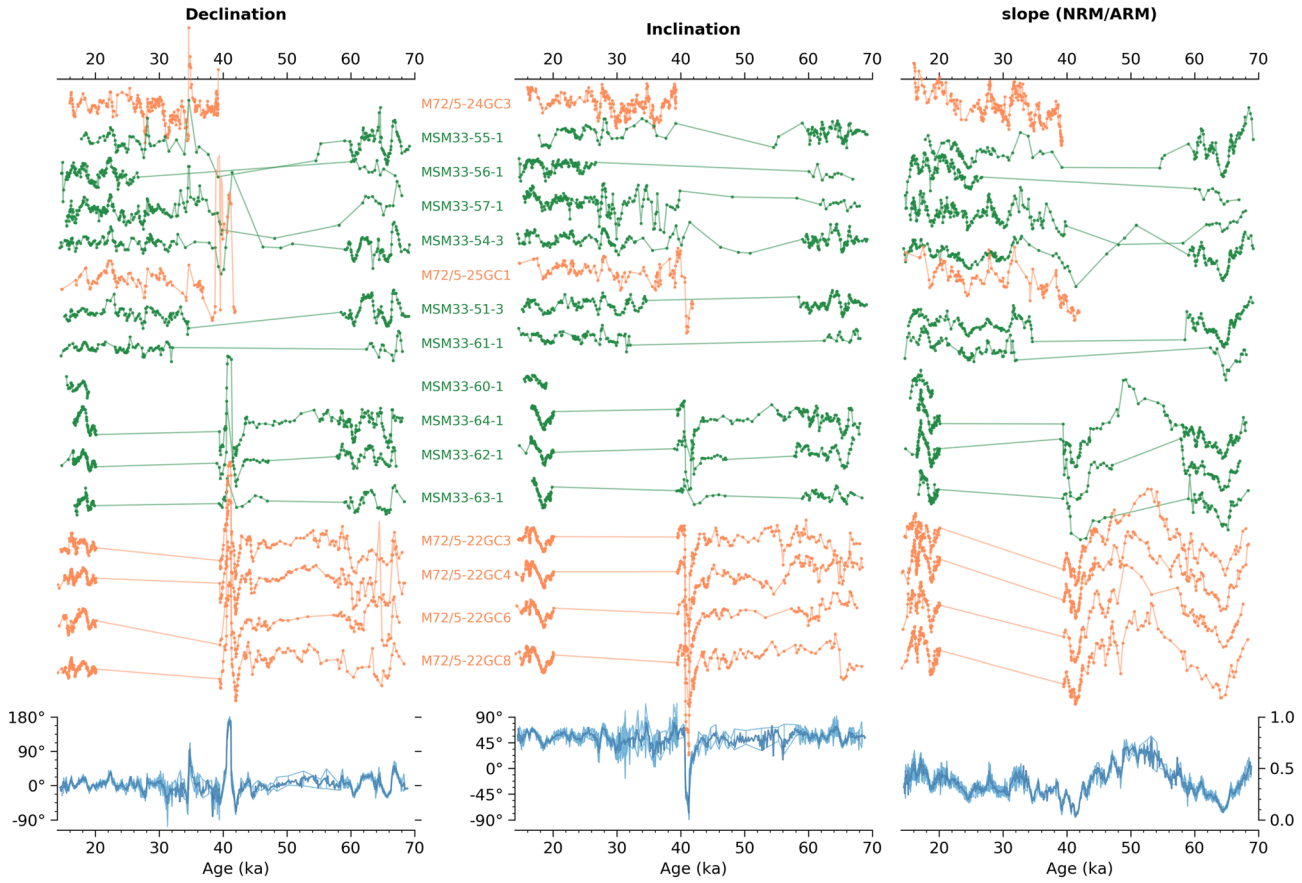

Figure 3. ChRM directions (declination and inclination) and relative paleointensity (rPI, approximated by the slope of NRM vs. ARM during AF demagnetization) are shown for 6 M72/5 cores (orange) and 10 MSM33 cores (green) for the time interval between 68.9 and 14.5 ka, together with their respective stacks (dark blue) at the bottom. For individual cores, ChRM directions and rPI are shown only for samples with SIRM/K_{LF} ratios ≤10 kAm^{-1}, empirically shown to omit greigite samples. Note that not all core sections shown here were used for stacking. For different time intervals, core intervals with directions differing from others are excluded from stacking; for example, Core M72/5-25GC1 is excluded from stacking between 42.6 and 39.44 ka due to a large number of greigite samples. Cores and number of samples used for stacking for different time intervals are given in detail in Table 1 and Figure 4. Inclination and declination were averaged together by Fisher (1953) statistics (supporting information Figure S6). Where available, the α_{95} for directional data (samples $n \geq 3$) and the 1σ standard deviation for relative palaeointensities (samples $n \geq 2$) are shown as vertical light blue bars. All individual records are plotted with a constantly increasing offset from core to core relative to their corresponding stacks. The cores are plotted from top to bottom according to their coring water depth (see Table 1) from shallow to deep.

24GC3, M72/5-25GC1, contain sediments from early MIS 5 back to middle/early MIS 6 (Shumilovskikh et al., 2013; Wegwerth et al., 2014, 2019) that are subject of ongoing comprehensive stratigraphic, paleomagnetic, and paleoenvironmental investigations.

3. Results

3.1. Compilation of the PSV Records From 68.9 to 14.5 ka

The Black Sea PSV record published by Nowaczyk et al. (2012, 2013) was based on six M72/5 cores. The improved record, supplemented by further 10 cores from the MSM33 expedition, is now based on 2,556 samples, almost doubling the number of included samples and providing directional data for the whole-time interval from 68.9 to 14.5 ka. Detailed descriptions of material and methods are given in supporting information Text S1. Demagnetization results from samples between 42.5 and 39.5 ka selected from Core M72/5-22GC8 are shown in supporting information Figure S5 (previously published by Nowaczyk et al., 2012). Here, the complete PSV record, comprising characteristic remanent magnetization (ChRM) directions (declination and inclination) and rPI (slope of natural remanent magnetization/anhysteretic remanent magnetization [NRM/ARM] during alternating field demagnetization) from all studied cores, is shown together with their stacks in Figure 3. For individual records, cores from Expeditions M72/5 and

MSM33 are plotted in orange color and green color, respectively. Stacked ChRM directions with the α_{95} error range (applying Fisher, 1953, statistics, see supporting information Figure S6) and rPI with 1σ standard deviation are plotted in the lower part of Figure 3. Note only for numbers of samples $n \geq 3$ ($n \geq 2$), α_{95} error bars (1σ error bars) are shown in the direction (rPI) stacks. The individual records are shown with constantly increasing offsets relative to their respective stacks.

In all studied Black Sea sediment cores, samples with SIRM/K_{LF} ratios >10 kAm^{-1} (SIRM: saturated isothermal remanent magnetization, K_{LF}: low-field magnetic susceptibility), empirically found to indicate the presence of diagenetically formed greigite, were omitted for paleomagnetic studies (Liu et al., 2018, 2019; Nowaczyk et al., 2012, 2018). Not necessarily the complete record of each individual core shown in Figure 3 was used for stacking. For the different time intervals, labeled with Roman numbers from I to V in Figure 4, cores with directions deviating from others are excluded from stacking. For example, data from Core M72/5-25GC1 are excluded from stacking between 42.6 and 39.44 ka due to an incomplete record caused by the exclusion of a large number of greigite-bearing samples (rock magnetic results of Core M72/5-25GC1 are given in Nowaczyk et al., 2012). The number of cores and number of samples used for stacking within different time interval are given in detail in Table 1 and Figure 4. Thus, a total of 2,556 out of 4,160, or 61.4% of all investigated discrete samples was considered for stacking for the time interval between 68.9 and 14.5 ka. The obtained Black Sea PSV stacks are shown in Figures 4a–4c. The available number of samples per time bin for the Black Sea PSV record is listed in Figure 4d. It is evident that from about 55 to 47 ka the directional stacks are less well defined (Figure 4). Due to the low data density, it was only possible to obtain α_{95} errors for a few mean paleomagnetic directions. Nevertheless, directions from consecutive samples, stacked together from five different cores, do not differ very much from each other (Figure 3). Thus, the obtained PSV record between about 58 and 42.5 ka appears fairly reliable and, therefore, is interpreted to represent geomagnetic field variations. The PSV stacks between 68.9 and 42.6 ka (Intervals V and IV; Figure 4) were calculated for 100-year time bins, as well as between 39.4 ka and 20 ka (Interval II; Figure 4). The PSV stacks spanning from 42.6 to 39.44 ka, covering the Laschamps excursion with a special high-resolution sampling protocol (supporting information Figure S1), could be calculated for 40-year time bins (Interval III; Figure 4). With plenty of samples, the PSV stacks between 20 ka and 14.5 ka were calculated for 50-year time bins (Interval I; Figure 4). The stacked records shown in Figures 3 and 4 comprise 649 time bins. Due to the lack of data in several intervals, 50 bins were interpolated linearly. In most cases only one value, for inclination, declination, and rPI each, had to be interpolated. Rarely two or three values were missing.

In the Black Sea PSV stacks (Figures 4a–4c), there is a deep minimum in the rPI at around 64.5 ka, associated with large swings in declination. Nowaczyk et al. (2018) interpreted these variations as a midlatitude expression of the geomagnetic excursion seen in sediments from northern high latitudes, the so-called "Norwegian-Greenland-Sea excursion" (e.g., Bleil & Gard, 1989; Løvlie, 1989; Nowaczyk & Frederichs, 1999; Nowaczyk et al., 2003; Xuan et al., 2012). Further on, the most prominent feature at around 41.2 ka, characterized by a short but full reversal and bracketed by a pronounced double low in rPI, was evidenced to be the Laschamps excursion by Nowaczyk et al. (2012, 2013). At about 34.5 ka, a swing in declination corresponding to the Mono Lake excursion was discussed by Liu et al. (2019). A well-defined minimum in inclination at around 18.5 ka, occurring within a minimum in rPI, is coeval with the postulated "Hilina Pali excursion" (e.g., Coe et al., 1978; Singer et al., 2014), though without excursional directions (Liu et al., 2018). There are further rPI minima values during the studied time interval, but without anomalous directions, indicating only normal secular variations.

3.2. Vector Transformation of the Black Sea PSV Record

The Black Sea rPI record (Figure 4a) was converted into virtual axial dipole moments (VADM) by comparison to data from the GEOMAGIA50 database (<50 ka, Brown et al., 2015) and from the International Association of Geomagnetism and Aeronomy (IAGA) Absolute Paleointensity (PINT) database (>50 ka, Biggin et al., 2010). A scaling factor of 14.52 was determined by the ratio of the average from absolute VADMs from databases to the average of rPI values from the Black Sea sediments (analogously to Nowaczyk et al., 2012). Thus, the Black Sea VADM values were obtained by applying this scaling factor to the rPI values. The field strength F was derived when the Black Sea VADM values were first divided by 8×10^{22} Am^2, the dipole moment from about CE 2000, and then multiplied by 48 μT, the field strength

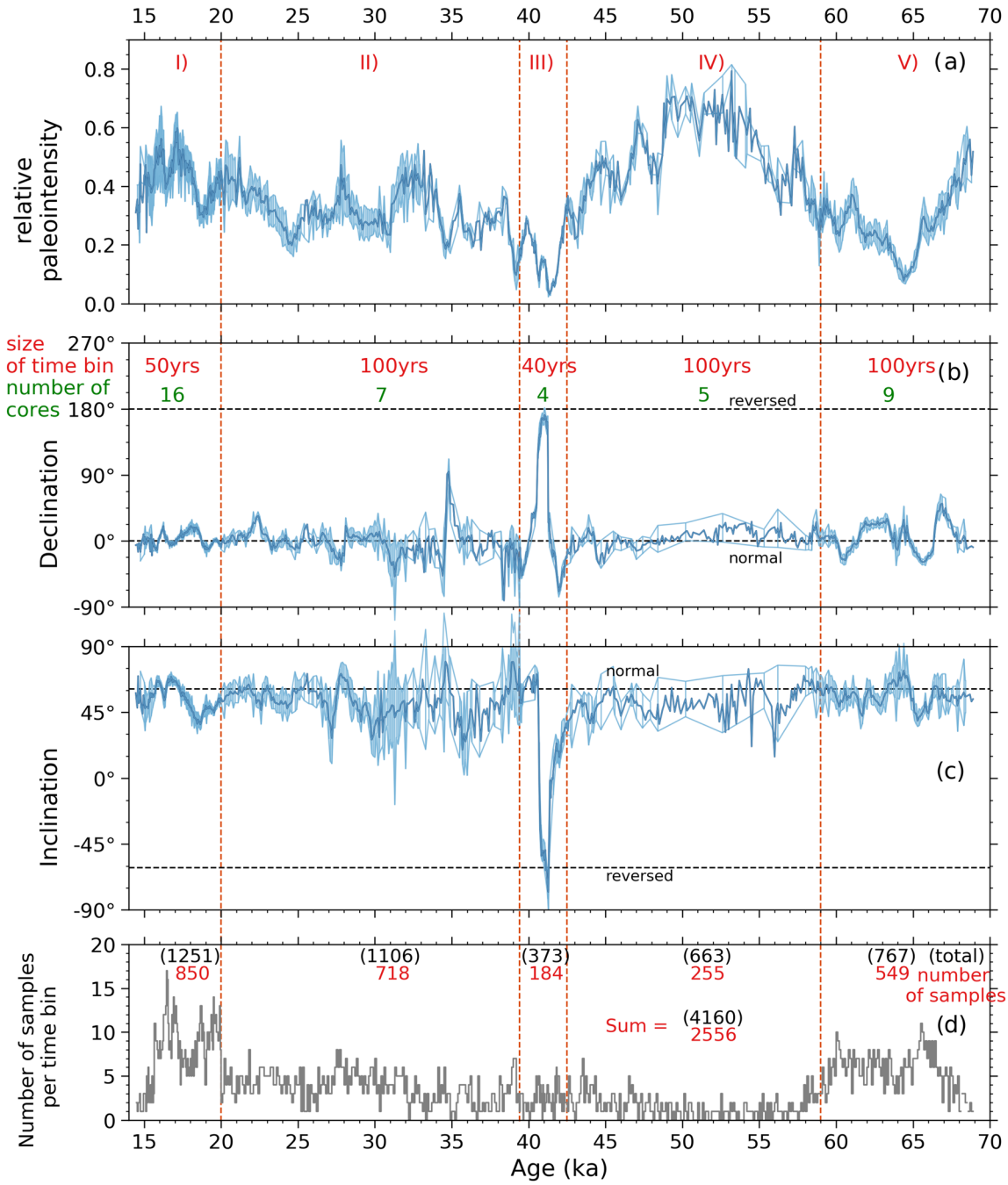

Figure 4. Summary of palaeomagnetic data obtained from a total of 16 sediments cores recovered from the SE Black Sea: (a) relative paleointensity (rPI), (b) declination, (c) inclination, and (d) number of samples per time bin. Where available, the 1σ standard deviation for relative palaeointensities (samples $n \geq 2$) in (a) and the α_{95} for directional data (samples $n \geq 3$) in (b) and (c) are shown in blue bars. Due to highly variable sedimentation rates and data coverage (cf. Figure 3), the record was divided into five subsections of different temporal resolution, labeled with roman numbers from I to V: I—Liu et al. (2018), II—Liu et al. (2019), III—Nowaczyk et al. (2012), IV—this study, and V—Nowaczyk et al. (2018). The temporal resolution (red numbers) and the number of sediment cores (green numbers) are indicated in (b), and the number of (investigated) used samples per subsection is given in (d) by (black) red numbers. The directions for a geocentric axial dipole field at the study site are indicated by blue dashed lines in (b) and (c).

for the SE Black Sea area (42°N, 37°E) in CE 2000 (according to the International Geomagnetic Reference Field, IGRF, https://www.ngdc.noaa.gov/geomag-web/?model=igrf). The absolute field strength F, together with Inclination I and Declination D, the geomagnetic field components given in spherical coordinates, was converted into Cartesian coordinates (X, Y, and Z), with $+X$ = north, $+Y$ = east, and $+Z$

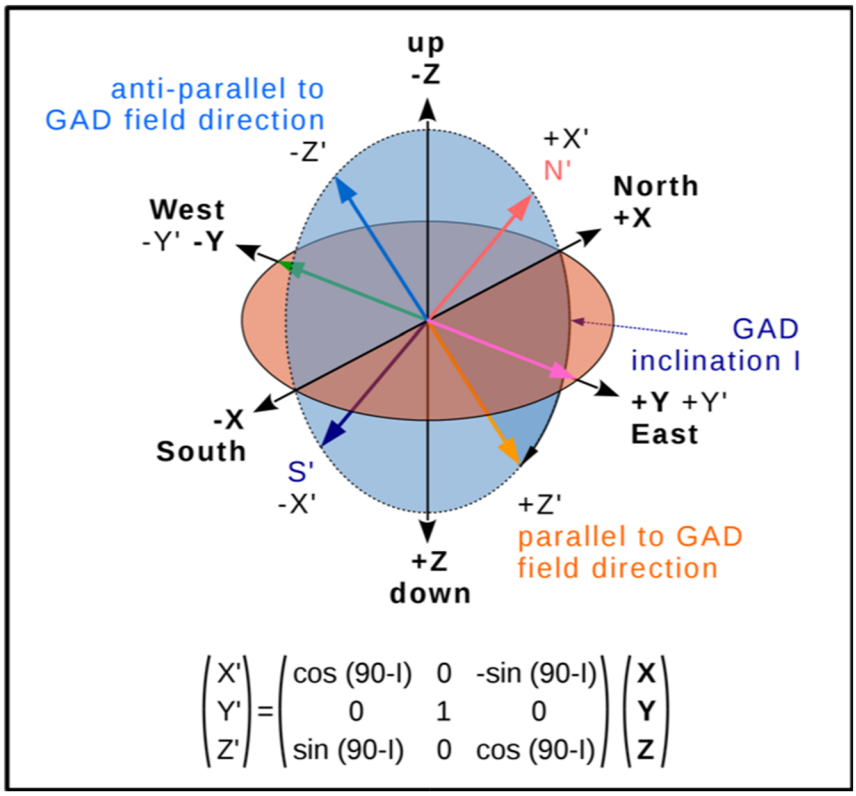

Figure 5. Sketch illustrating the coordinate transformation performed on the Black Sea paleosecular variation record. Paleomagnetic data recalculated to Cartesian coordinates (X, Y, and Z, see section 3.2) were rotated around the Y axis (EW) so that the obtained Z' component is parallel to the field direction of a geocentric axial dipole (GAD) of normal polarity with an Inclination I of 61° (latitude of 42°N). The transformation matrix is shown in the lower part of the sketch. The obtained X' and Y' components then are definitely field contributions only from nondipole components.

pointing downward (Figure 5). In a final step, data were transformed into a rotated Cartesian coordinate system (X', Y', and Z') as laid out in the matrix equation in Figure 5. Now, Z' is parallel to the expected field direction of a GAD at the study site (42°N, 37°E). Thus, PSVs in X' (tilted NS) and Y' (=Y, EW) are then definitely related only to nondipole contributions to the geomagnetic field. However, zonal harmonics, due to their rotational symmetry, do not contribute to the Y′ (EW) component. Although Z' is parallel to the GAD field line, this component can also comprise contributions from higher-order multipoles.

A similar coordinate transformation of paleomagnetic data was suggested by Hoffman (1984) as an alternative to the evaluation of intermediate directions on the basis of VGPs. However, in contrast to Hoffman (1984), we do not use only inclination and declination (normalized directions) but the full vector, including intensity. In addition, our main goal is to gain some insight into the field dynamics in terms of intensity variations across excursions and the overall geometry of the field (simple/complex).

The transformed field vector components (X', Y', and Z') from the Black Sea paleomagnetic stacks are shown in Figures 6a–6c. The frequency distributions of the three transformed field vectors (X', Y', and Z') are shown together with the inclination distribution in supporting information Figure S7. There appears to be a persistent trend in the X' component for more positive than negative values (Figures 6a and S7a). This is due to inclinations being persistently lower (by about 10°) than the inclination of 61° expected from a pure GAD field at the Black Sea site. One likely explanation is inclination shallowing during compaction of the mainly siliciclastic sediments. A similar effect is being observed in resedimentation experiments with the studied Black Sea sediments under controlled field conditions (work in progress). In contrast, the variation of Y', the E/W component, does not show any offset (Figures 6b and S7b). This is caused by the fact that cores were taken without azimuthal orientation and that a subsequent reorientation was performed by mathematically correcting ChRM declinations of each core to zero mean. From 68.9 to 14.5 ka, the X' and Y' components

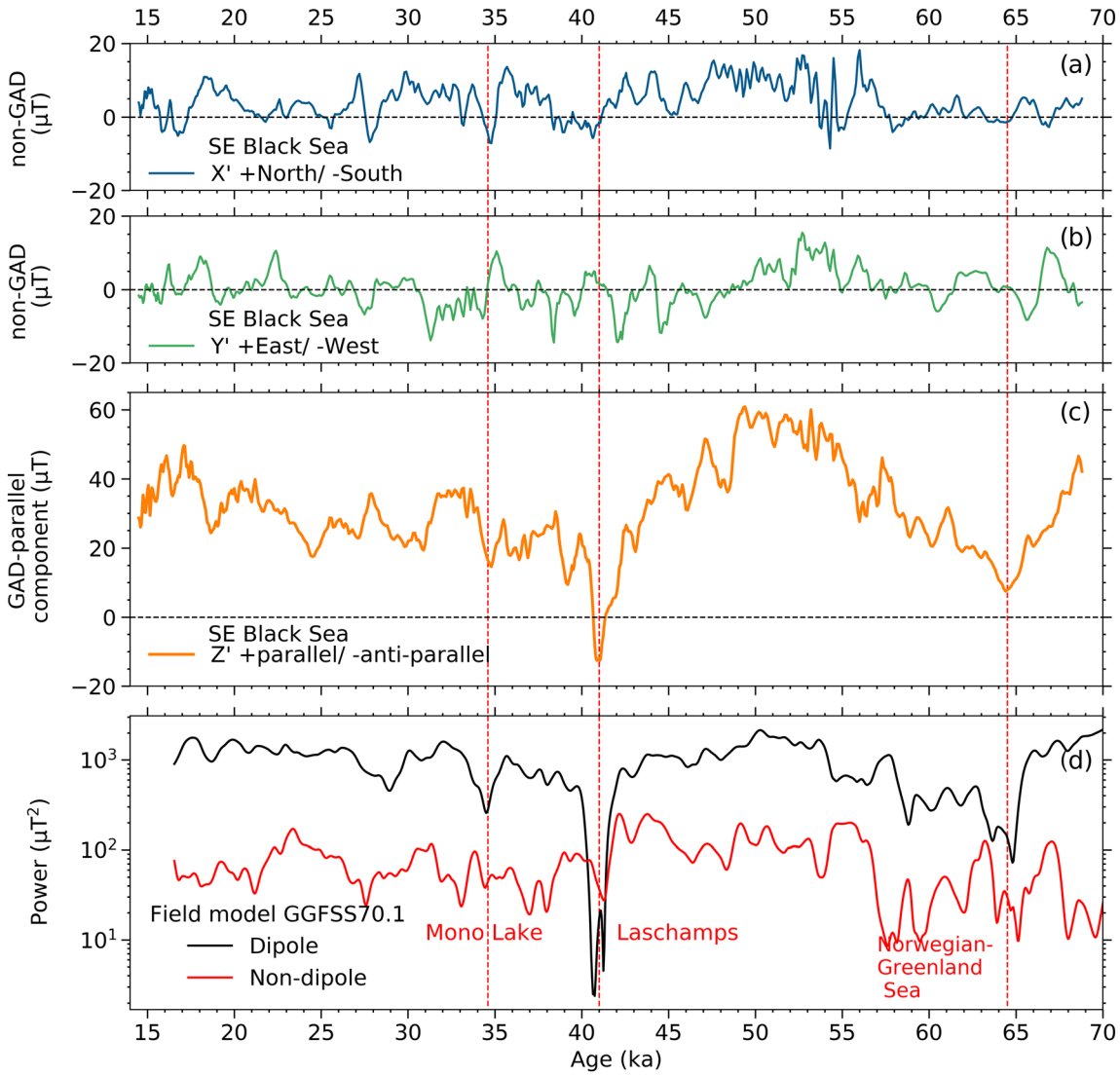

Figure 6. Field components perpendicular to the direction of a pure geocentric axial dipole (GAD) defined as non-GAD components (a) along NS (X') and (b) parallel EW (Y'), and (c) GAD-parallel component (Z') calculated from the Black Sea paleomagnetic record (see Figure 5). (d) Dipole (black) and nondipole (red) power evolutions on the Earth surface derived from the Model GGFSS70.1 constrained by the Black Sea PSV stacks and five other globally distributed records (for details refer to section 3.3). Note that in Figure 6d the power of the dipole component, with squared amplitudes, is plotted on a log scale.

display fairly constant oscillation amplitudes between −10 and +10 mT across excursions and intervals of normal secular variations (Figures 6a and 6b). On the other hand, the Z' component shows extremely low values at about 65 and 41 ka (Figure 6c). Specifically, negative values of the Z' component are exclusively observed at about 41 ka, which is coeval with the Laschamps excursion. Between about 65 and 41 ka, the Z' component reached the highest values of ~60 μT centered at about 52 ka. After the Laschamps excursion, the Z' component is gradually increasing from 40 to 15 ka, though it does not recover to its pre-Laschamps maximum strength. The Mono Lake excursion at about 34.5 ka is simply characterized by a relatively low Z' component.

In Figure 6d, the dipole and nondipole power on Earth surface are shown for the Geomagnetic Field Model GGFSS70.1 (Global Geomagnetic Field model from Selected Sediments for the past 70 ka). The GGFSS70.1 model, spanning the period 70–15 ka, is based on the modeling method described by Panovska, Constable, and Korte (2018). A temporally continuous geomagnetic field model is obtained by an inversion using spherical harmonic functions in space (maximum Degree 6), cubic B-splines in time (with a time knots spacing of 50 years) and all records equally weighted. The model is constrained by six high-resolution paleomagnetic

records from globally distributed sites: the Black Sea PSV stacks (data from this study), data from Core JPC-14, North Atlantic Ocean (Lund et al., 2001, 2005), Site ODP-1233, Chile Margin, SE Pacific (Lund, Stoner, & Lamy, 2006; Lund et al., 2007), Core MD94-103, southern Indian Ocean (Mazaud et al., 2002), Core MD98-2181, western equatorial Pacific Ocean (Lund, Schwartz, et al., 2017), and Core PLC08-1, Pyramid Lake, USA (Lund, Benson, et al., 2017). New age models were derived for Site ODP-1233 (Chase et al., 2014) and Core MD94-103 records (Sicre et al., 2005). From this limited but highly improved data set including only high-quality records with good age controls, we derived a model with a better temporal resolution and more consistent global variations. Therefore, this new model is used for comparisons here instead of a published and more smoothed model covering this timescale, the GGF100k (Global Geomagnetic Field over the past 100 ka) (Panovska, Constable, & Korte, 2018).

In Model GGFSS70.1, between 68.9 and 57 ka, the nondipole power is low, but oscillating over 1 order of magnitude (note the log scale) (Figure 6d). According to this, the Black Sea X' and Y' (non-GAD) components vary in a narrow range of about ±5 mT between about 67 and 57 ka (Figures 6a and 6b). Further on, spanning from 55 to 14.5 ka, both the Black Sea X' and Y' components and the nondipole field in Model GGFSS70.1 exhibit fairly stable oscillation in a fairly narrow range. Thus, fluctuations in Black Sea X' and Y' components, related only to nondipole contributions, are characterized by comparable variations like those of the nondipole component in Model GGFSS70.1. On the other hand, the dipole power in Model GGFSS70.1 exhibits generally high amplitudes during normal secular variations and fairly low amplitudes crossing the Norwegian-Greenland Sea, the Laschamps, and the Mono Lake excursions (Figure 6d). The Black Sea Z' component (Figure 6c), parallel to the GAD field, displays a change coherent with that of the dipole field in GGFSS70.1 (Figure 6d). Nevertheless, the Z' component derived from Black Sea PSV record also comprises contributions from higher-order multipoles and presents more fluctuations.

3.3. Field Strength, VGP Positions, and PSV Index

In Figures 7a–7c, the X', Y', and Z' components derived from the Black Sea PSV record are shown together with the total field strength in Figure 7d, the associated VGP latitudes in Figure 7e, and the PSV index P_i, defined by Panovska and Constable (2017), in Figure 7f. The decay and growth rates of field strength were estimated for the Norwegian-Greenland Sea, the Laschamps, and the Mono Lake excursions using 1° polynomial curve fitting (Figure 7d). Toward the Norwegian-Greenland Sea excursion, the field strength at the Black Sea site was continuously decreasing at a rate of about −8.2 nT/year between 68.9 and 64.5 ka. Then the field strength was steadily growing at a rate of about +5.3 nT/year from 64.5 to 61 ka and finally peaked at about 52 ka. For a better inspection, the complex field variations between 45 and 30 ka across the Laschamps and the Mono Lake excursion, are also shown in more detail in Figure 8. During the Laschamps excursion, the decay rate of −19.9 nT/year of the Black Sea field strength and the recovery rate of +11.5 nT/year are comparable with those estimated from the GLOPIS75 (Laj & Kissel, 2015; Laj et al., 2014). Nevertheless, during the onset of the Laschamps excursion, a much higher decay rate of −30.2 nT/year is estimated in the Black Sea field strength between 42.5 and 41.6 ka (Figure 8b). Then the Black Sea field strength also recovered (with reversed directions) at a higher rate of about +30.3 nT/year after 41.2 ka (Figure 8b). After the Laschamps excursion's fully reversed phase ended at 40.6 ka, the Black Sea field strength was growing at a rate of +20.2 nT/year (Figure 8b). Between 35.5 and 34 ka, during the Mono Lake excursion, the decay and growth rates of the Black Sea field strength was estimated to be −17.6 and +24.3 nT/year, respectively.

The Laschamps and the Mono Lake excursions are evidenced by VGPs moving to latitudes lower than 45°N, commonly defined as excursional behavior (Laj & Channell, 2015), with the Laschamps excursion reaching even high southern latitudes (Figure 7e). In the Black Sea record, some single VGPs reach latitudes as low as 45°N at about 38.2 and 31.2 ka. However, they were calculated from directional data with larger α_{95} values as shown in Figure 4 and thus comprise some uncertainties. The PSV index P_i is an activity index for evaluating geomagnetic secular variations, excursions, and reversals. For a stable geomagnetic field configuration, dominated by an axial dipole, the P_i calculates to values ≤0.3. On the other hand, geomagnetic excursions, conventionally defined by VGP latitudes being lower than 45°N and a dipole moment of maximum half of the present day value, would give P_i values ≥0.5 (Panovska, Constable, & Brown, 2018). In Figure 7f, the P_i calculated from the Black Sea PSV record is shown together with the globally averaged P_i from the sediment records in the 100-ka data compilation (Figure 8 in Panovska, Constable, & Brown, 2018). In the Black

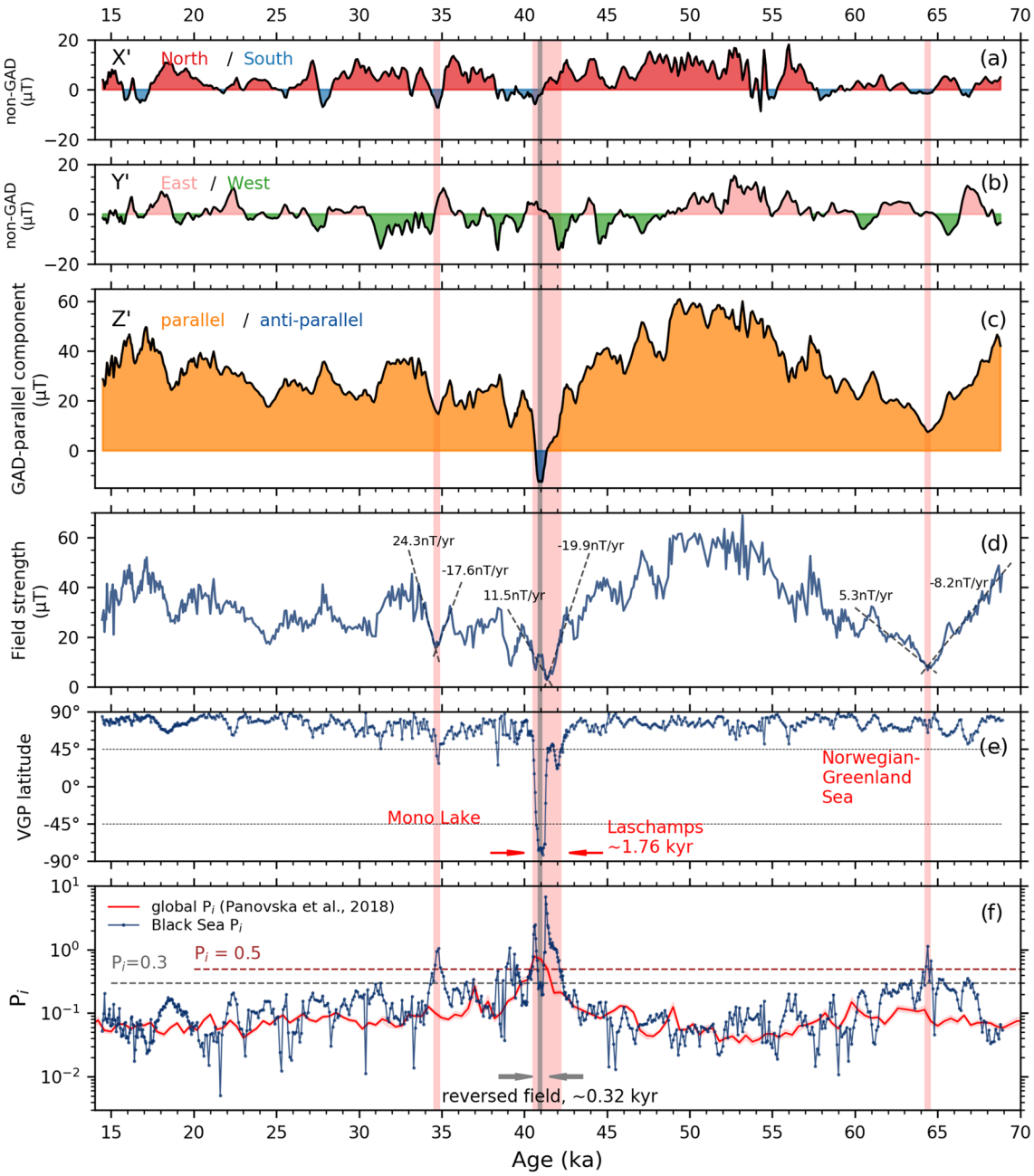

Figure 7. Paleosecular variation record from Black Sea sediments spanning from 68.9 to 14.5 ka. (a) X′ component and (b) Y′ component representing solely nongeocentric axial dipole (non-GAD) contributions. (c) Z′ component parallel to the field direction of a GAD of normal polarity (see Figure 5). For comparison, the original data sets obtained are shown as (d) field strength and (e) latitude of the related virtual geomagnetic pole (VGP). In (d), the decay and growth rates of field strength F indicated by gray dashed lines were determined from the slope of field strength F using 1° polynomial curve fitting. (f) The paleosecular variation (PSV) index P_i, calculated from the Black Sea paleomagnetic data (in blue) and determined from global paleomagnetic records (in red, Panovska, Constable, & Brown, 2018). A stable (excursional) geomagnetic field is indicated by values of $P_i \leq 0.3$ ($P_i \geq 0.5$). The Norwegian-Greenland Sea, the Laschamps, and the Mono Lake excursions, indicated by vertical red bars, are characterized by excursional $P_i > 0.5$. Nevertheless, only the Laschamps excursion and the Mono Lake excursion were found to show VGP latitudes moving lower than 45°N (Figure 8). The reversed polarity during the Laschamps excursion, marked by the vertical gray bar, is indicated by a negative GAD-parallel component and VGPs with latitudes higher than 70°S.

Sea P_i record, during the Norwegian-Greenland Sea, the Laschamps, and the Mono Lake excursions, the geomagnetic field is ubiquitously characterized by P_i values ≥0.5, whereas the globally averaged P_i exhibits fairly smoothed variations (because of the stacking of more than 100 records), with P_i values ≥0.5 only during the Laschamps excursion. For the time intervals from 60 to 43 ka and from 30 to 14.5 ka, the

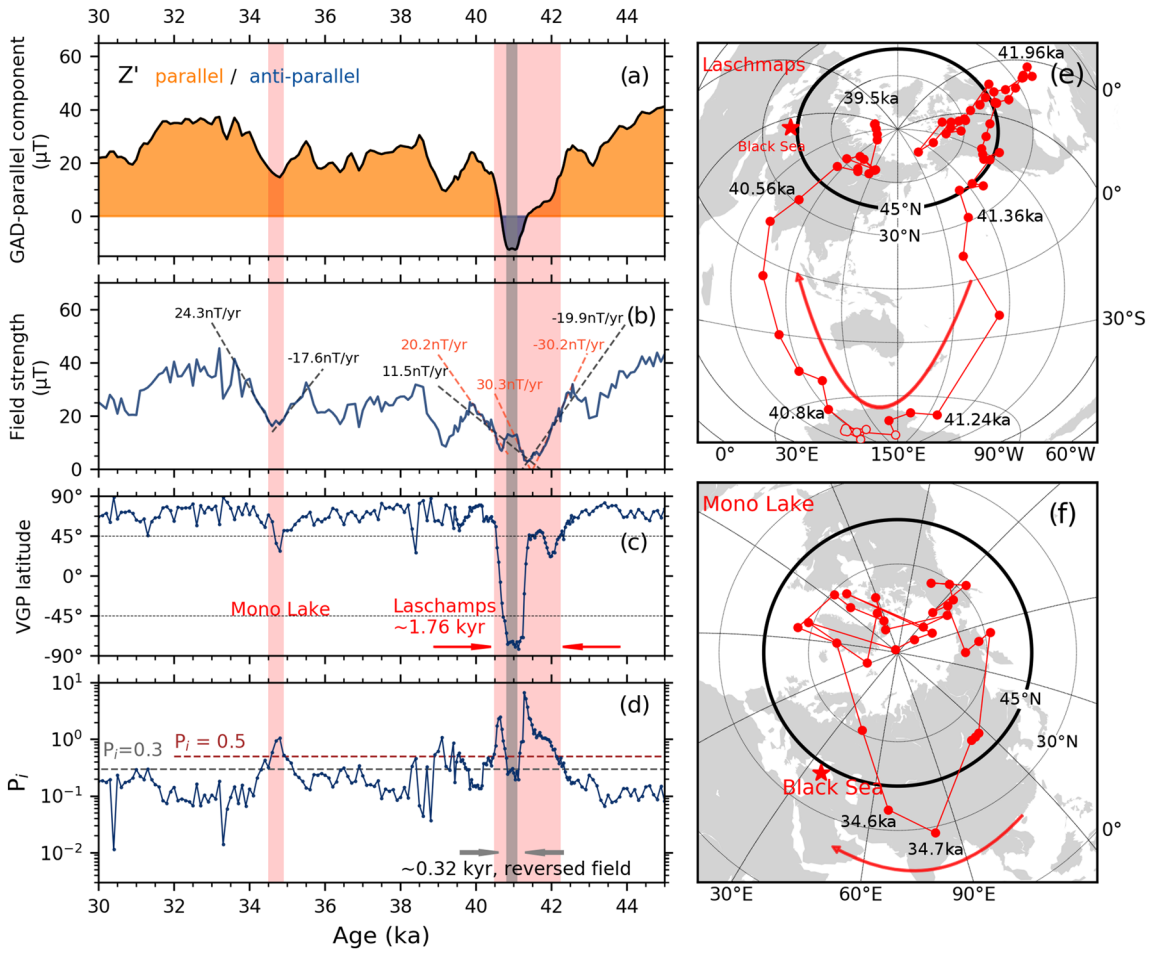

Figure 8. (a–d) Close-up view of the paleosecular variation record from Black Sea sediments spanning from 45 to 30 ka, covering the Laschamps and the Mono Lake excursions (see also Figure 7). (a) Component (antiparallel) parallel to the field of a geocentric axial dipole (GAD; see Figure 5). (b) Reconstructed field strength. (c) Virtual geomagnetic pole (VGP) latitude. (d) Paleosecular variation (PSV) index P_i, indicating stable (excursional) geomagnetic field with values of $P_i \leq 0.3$ ($P_i \geq 0.5$). VGP paths derived from Black Sea sediments are shown during (e) the Laschamps excursion and (f) the Mono Lake excursion. The VGP paths of the Laschamps excursion and the Mono Lake excursion have temporary resolutions of 40 and 100 years, respectively. VGPs of the reversed field during the Laschamps excursion are indicated by hollow circles in Figure 8e.

Black Sea P_i record implies stable normal secular variations with P_i values being persistently <0.3 (Figure 7f) and VGPs latitudes higher than 45°N (Figure 7e).

In Figure 9, VGP paths derived from Black Sea sediments are shown for the Norwegian-Greenland Sea excursion, the Laschamps excursion, the Mono Lake excursion and the time interval contemporary to the postulated "Hilina Pali" excursion. During the Norwegian-Greenland Sea excursion, VGPs between 69 and 64 ka were quickly changing positions between opposite sides of the globe (Northern America and Siberia) almost reaching excursional latitudes (Figure 9a). During the Laschamps excursion, VGPs first moved from the Arctic to the Sargasso Sea (15°N) in the North Atlantic at about 41.96 ka then migrated northwest to Northern America (Figures 8e and 9b). Between 41.5 and 40.5 ka, the Black Sea VGPs performed a clockwise loop crossing the central Pacific Ocean, reaching the Antarctic continent, and then migrating back to the Arctic via the India Ocean (Figures 8e and 9b). After this main loop of the Laschamps excursion, the Black Sea VGPs swung to the Labrador Sea with almost transitional VGP latitudes again at about 39.5 ka (Figures 8e and 9b). During the Mono Lake excursion, the Black Sea VGPs first were moving from Alaska to southern Asia (30°N) then crossing central Asia and moving back to Greenland (Figures 8f and 9c). The postulated "Hilina Pali excursion," centered at about 18.5 ka, shows no abnormal VGP positions in the Black Sea record (Figure 9d).

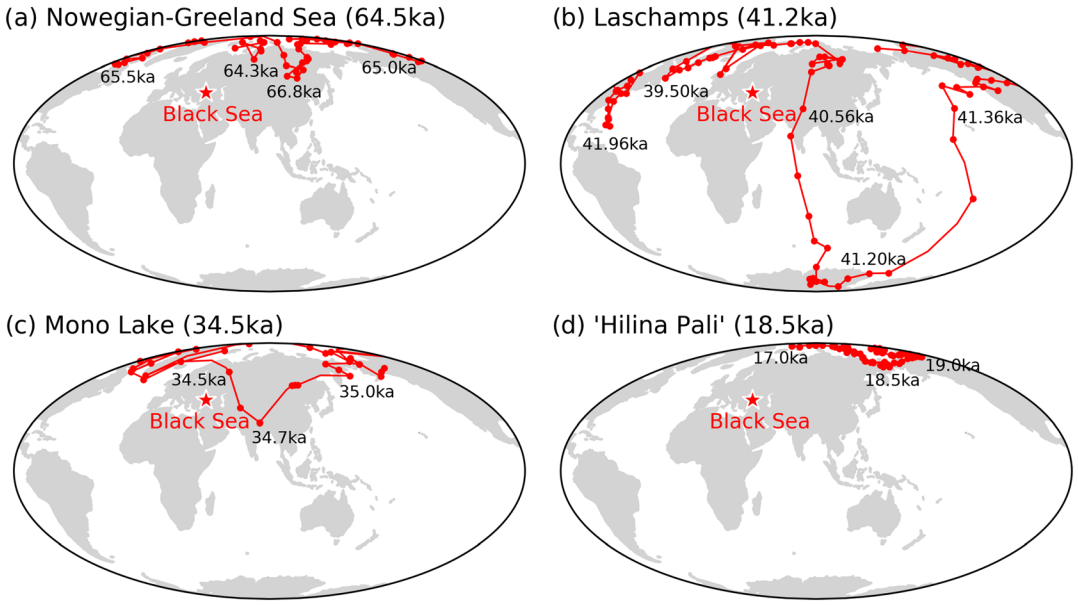

Figure 9. Virtual geomagnetic pole (VGP) paths calculated from the Black Sea paleomagnetic directional stacks (see Figure 4). (a) VGPs between 69 and 64 ka, covering the Norwegian-Greenland Sea excursion. (b) VGPs between 43 and 39 ka, covering the Laschamps excursion. (c) VGPs between 36 and 33 ka, covering the Mono Lake excursion. (d) VGPs between 20 and 17 ka, covering the postulated "Hilina Pali excursion."

4. Discussion

4.1. The Norwegian-Greenland Sea Excursion (~64.5 ka)

The Norwegian-Greenland Sea excursion, in the Black Sea record, is characterized by positive shallow to steep inclinations and large swings in declination. It has been first reported from the Arctic, that is, from the Kolbeinsey Ridge (Bleil & Gard, 1989; Løvlie, 1989; Nowaczyk & Frederichs, 1999), the Fram Strait (Nowaczyk et al., 2003), the Yermak Plateau (Nowaczyk & Baumann, 1992; Xuan et al., 2012), and the Baffin Bay (Simon et al., 2012). Recent studies on cores from the Arctic Ocean (e.g., Mendeleev-Alpha Ridge, Lomonosov Ridge, and Yermak Plateau) postulate a self-reversed chemical remanent magnetization (CRM) carried by titanomaghemite formed during seafloor oxidation of host (detrital) titanomagnetite grains, which could also produce shallow and negative inclinations (Channell & Xuan, 2009; Xuan & Channell, 2010; Xuan et al., 2012). Wiers et al. (2019) further evidenced the influence of seafloor oxidation on paleomagnetic records from the Arctic Ocean can vary in time and space. On the other hand, in Core MD98-2181 from the west equatorial Pacific Ocean, Lund, Schwartz, et al. (2017) found abnormal directions that can be associated with the Norwegian-Greenland Sea excursion. This is the first recognition of this event outside the Arctic area. Nevertheless, Lund, Schwartz, et al. (2017) pointed out that the data are not truly excursional and the recorded directions should be considered as a tentative assignment to the Norwegian-Greenland Sea Excursion. Thus, the overall field configuration during the (postulated) Norwegian-Greenland Sea excursion is not yet well defined.

Anyway, the remarkable field intensity low at 64.5 ka, coeval with the Norwegian-Greenland Sea excursion, is observed in many records from globally distributed sites (e.g., Laj et al., 2004; Lund, Stoner, Channell, et al., 2006; Thouveny et al., 2004). Especially in the Black Sea PSV record, the Norwegian-Greenland Sea excursion is expressed as the second deepest intensity minimum ($F = 8$ μT) during the past 70 ka (Figure 7d). Fairly low long-term decay and growth rates (−8.2 and 5.3 nT/year, respectively) can be observed across the Norwegian-Greenland Sea excursion, thus making it a broad minimum in the Black Sea field strength record. Accordingly, the GAD-parallel component (Z') also dropped significantly down to 7.5 μT at about 64.5 ka (Figure 7c), likely indicating a deep low in the axial dipole field contribution. Although no excursional VGP latitudes (≤45°N) were observed (Figure 7e), the extremely low GAD-parallel component (Z') and total field strength during the Norwegian-Greenland Sea excursion are corresponding to P_i values ≥0.5, indicative for geomagnetic excursions (Figure 7f). Besides this, the VGPs

derived from Black Sea sediments between 69 and 64 ka exhibit quickly changing positions between opposite sides of the globe almost reaching excursional latitudes (Figure 9a; Nowaczyk et al., 2018). The non-GAD components, particularly the X' component, in the Black Sea record show fairly weak fluctuations between about 67 and 57 ka (Figures 7a and 7b). In addition, a simultaneous and significant decay of both the dipole and nondipole field is seen in the GGFSS70.1 model summarizing global data (Figure 6d). After 64.5 ka, the strong similarity in the increase of Black Sea GAD-parallel component and total field strength, finally peaking at about 52 ka (Figures 7c and 7d), clearly indicates the recovery of the dipole field contribution. This is also confirmed by the GGFSS70.1 model (Figure 6d).

Nevertheless, the postulated questionable fidelity of paleomagnetic records from the Arctic Ocean suggested by Wiers et al. (2019), on the other hand, the low field intensities in concert with fast changing direction reliably determined from the SE Black Sea (Nowaczyk et al., 2018), need further investigations at other sites on the globe in order to decipher the real field configuration during the Norwegian-Greenland Sea excursion.

4.2. The Laschamps Excursion (~41.2 ka)

The Laschamps is the best-known geomagnetic excursion in the Brunhes Chron (see review by Channell et al., 2020). Centered at about 41 ka, extremely low field intensities and excursional VGPs (≤45°N) associated with the Laschamps excursion have been commonly reported from global sites (e.g., Bonhommet & Babkine, 1967; Cassata et al., 2008; Ingham et al., 2017; Lund, Stoner, Channell, et al., 2006; Plenier et al., 2007). In the Black Sea PSV record, the Laschamps excursion is characterized by the lowest (total) field intensity estimates of down to $F = 3$ μT (Figure 8d) during the N-R transition, VGPs reaching nearly 80°S (Figure 8e), and $P_i \geq 0.5$ (Figure 8f). In this main phase of the Laschamps excursion recorded in Black Sea sediments, associated VGPs perform a clockwise loop migrating south through the central Pacific, crossing the Antarctica, and back North through the central Indian Ocean (Figures 8e and 9b). First, this appears to be in agreement with the findings of Laj et al. (2006). Based on seven high-resolution sedimentary records (separated by 178° of longitude and 113° of latitude) and U-channel measurements, Laj et al. (2006) postulated a simple clockwise VGP loop passing south through the western Pacific and back north through Africa as the typical field behavior for the Laschamps excursion. They proposed that the consistency among the VGP paths from different sites results from equatorial dipole contributions and a reduced nondipole field during the excursion. However, this scenario of the Laschamps excursion is an oversimplification (Roberts, 2008) and likely the result of significant time averaging of U-channel measurements (e.g., Philippe et al., 2018). Most VGPs of the Laschamps excursion derived from lava flows (e.g., Cassata et al., 2008; Ingham et al., 2017; Plenier et al., 2007) do not lie close to the clockwise loop of Laj et al. (2006). Especially the Black Sea VGP path during the Laschamps excursion (Figures 8e and 9b) disagrees with the VGP path claimed by Laj et al. (2006), but it is in agreement with the VGPs from the volcanic at the type locality in France (see Figure 8 in Nowaczyk et al., 2012). In addition, excursional VGPs during the early phase of the Laschamps excursion at about 42 ka first migrate to the Sargasso Sea in the North Atlantic (15°N, Figures 8e and 9b), a feature also seen to some degree in the paleomagnetic record from ODP Site 1063 (Bermuda Rise) investigated by Channell et al. (2012). Only then, after crossing North America, Black Sea VGPs perform a loop through the Pacific but further to the east. After this loop, there is also another swing into the Atlantic sector with VGPs reaching the Labrador Sea at around 39.5 ka with almost transitional VGP latitudes (Figures 8e and 9b). Thus, the Laschamps excursion was definitely a much more complex feature than postulated by Laj et al. (2006).

The Black Sea PSV index P_i indicates that the Laschamps excursion comprises even a "normal secular variation" interval during its fully reversed phase ($P_i \leq 0.3$), bracketed by the two polarity transitions ($P_i > 0.3$, Figure 8d). The "normal secular variation" interval characterized by VGPs sited in the Antarctic continent (hollow circles in Figure 8e), therefore, represents an extremely short subchron of reversed polarity. This time interval, spanning from about 41.16 to 40.84 ka, is marked with a gray bar in Figures 7 and 8. The two transitional intervals, corresponding with N → R and R → N transitions of VGPs (Figure 8e), are marked with red bars for the time windows of 42.24–41.16 and 40.84–40.48 ka (Figures 7 and 8), respectively. Thus, based on VGPs ≤ 45°N and $P_i > 0.3$, the full duration of the Laschamps excursion documented in the Black Sea PSV record can be estimated to be about 1.76 kyr, including an interval of about 0.32 kyr of fully reversed polarity. Age uncertainties were estimated for individual Black Sea cores using *Undatable* (Lougheed & Obrochta, 2019) shown in Figure 2e. Between about 39.4 and 42.6 ka, the D-O Events 9–10 are clearly

recognized in the Black Sea IRD counts and Ca/Ti and K/Ti records that can be well correlated to the NGRIP $\delta^{18}O$ record (supporting information Figures S2–S4), thus yielding limited age uncertainties (Figure 2e).

During the N → R transition of the Laschamps excursion, it is noteworthy that the GAD-parallel component and total field strength were plunging to about 0 μT (changing sign toward negative values) and 3 μT, respectively (Figures 8a and 8b). Specifically, the decay rate of field strength of −30.2 nT/year during the onset of N → R transition (Figure 8b) is about 2 times higher than previously estimated for the onset of the Laschamps excursion (Laj et al., 2014; Laj & Kissel, 2015). It is also interesting to note that the onset of the fully reversed phase is characterized by a high growth rate of the field strength of +30.3 nT/year (Figure 8b). The reversed polarity phase of the Laschamps excursion is characterized by a negative GAD-parallel component of about −12 μT (Figure 8a) and a fairly high total field strength of 12.5 μT (Figure 8b). During the R → N transition of the Laschamps excursion, the negative GAD-parallel component approached low positive values (Figure 8a), and the total field strength declined slightly to about 7.5 μT and then increased later at a growth rate of +20.2 nT/year (Figure 8b). This more complex directional and paleointensity structure of the Laschamps excursion, with a double paleointensity minimum, has also been documented in other high-resolution sedimentary records, for example, Core MD95-2034 (Bermuda Rise, Laj et al., 2000), Core PS2138-1 (Arctic Ocean, e.g., Nowaczyk & Knies, 2000), Core ODP-1233 (Chile Margin, Lund et al., 2007; Lund, Stoner, & Lamy, 2006), and Core MD07-3076Q (South Atlantic mid-ocean ridge, Channell et al., 2017). Nevertheless, it is difficult to recover the short-lived polarity reversal of the Laschamps in most other sediments due to low sedimentation rates (Roberts & Winklhofer, 2004; Valet et al., 2016) and/or U-channel sampling (Philippe et al., 2018).

Leonhardt et al. (2009) argued that the dynamic nondipolar components lead to considerable deviations among predicted records at different locations, though the dipolar field at the Earth's surface was dominant during the Laschamps excursion. On the other hand, Korte et al. (2019) suggested that the axial dipole decayed extremely to a level where the nondipole field dominates at the Earth's surface during the Laschamps excursion, though the nonaxial dipole field remain relatively unchanged (Korte et al., 2019; Wicht & Meduri, 2016). In the Black Sea PSV record, the negative GAD-parallel component, with relatively high total field strength, VGPs higher than 70°S and a $P_i < 0.3$ (Figures 8a–8d) during the reserved polarity phase of the Laschamps excursion, indicate the development of an axial dipole field in opposite direction. Although the reversed axial dipole field was not that strong (GAD-parallel component = ~ −12 μT) and short-lived (~0.32 kyr), it was responsible for the reversed VGPs located at high southern latitudes, also observed at other globally distributed sites. This is consistent with findings from simulations by Valet and Plenier (2008) and Brown and Korte (2016) that a reversed axial dipole with a certain strength is required to produce (globally) reversed directions, and consequently VGP positions at high southern latitudes. During the N → R (R → N) transition of the Laschamps excursion, both the GAD-parallel component and the total field strength in the Black Sea PSV record exhibit a significant decrease (increase). The variations of the GAD-parallel component are mostly consistent with the decay and recovery of the dipole field observed in geomagnetic field models covering the Laschamps excursion (Brown et al., 2018; Korte et al., 2019), as well as in the model GGFSS70.1 (Figure 6d).

Thus, the Black Sea PSV record reflects rapidly changing field configurations across different phases of the Laschamps excursion. The GAD-parallel component derived from the Black Sea PSV record imply a decay of the axial dipole field during the N → R transition phase, development of an axial dipole field in opposite direction during the reversed polarity phase, and then a recovery of the normal axial dipole field configuration during the R → N transition phase, but without noticeable variations of the nondipole field contributions seen in the non-GAD components and the nondipole component of GGFSS70.1. After the Laschamps excursion, the Black Sea GAD-parallel component and field strength was slightly increasing and did not reach half of their pre-Laschamps strength until about 35 ka (Figures 7c and 7d). In addition, the post-Laschamps Black Sea PSV index P_i shows some values ≥0.3 (Figure 8d), indicating the magnetic field remained unstable until the Mono Lake excursion discussed in the next section.

4.3. The Mono Lake Excursion (~34.6 ka)

The Mono Lake excursion, distinct from the Laschamps excursion, has been cumulatively documented in both sedimentary and volcanic records (e.g., Cassata et al., 2008; Channell, 2006; Kissel et al., 2011; Lund et al., 1988; Lund, Benson, et al., 2017; Ménabréaz et al., 2011; Negrini et al., 2014; Nowaczyk &

Knies, 2000). During the Mono Lake excursion, low intensities coeval with abnormal directions are commonly identified. However, comparison of available paleomagnetic data from global sites reveals diverging VGP paths of the Mono Lake excursion for the individual sites, and thus, no satisfactory field configuration could be concluded (Kissel et al., 2011). By comparing the VGPs from different sites, Negrini et al. (2014) suggested a time-transgressive decay and return of the principal field components at the beginning and the end of the Mono Lake excursion, respectively, leaving the nonaxial dipole dominant during the excursion.

In the Black Sea PSV record, the Mono Lake excursion at about 34.5 ka shows medium low field intensities (F = ~17.5 μT), excursional VGP latitudes (≤45°N), and P_i values >0.5 (Figures 7 and 8). A decay rate of −17.6 nT/year and a recovery rate of +24.3 nT/year, observed in the Black Sea field strength across the Mono Lake excursion, are in agreement with the changing rates estimated from GLOPIS-75 by Laj and Kissel (2015). During the Mono Lake excursion, the Black Sea VGPs moved clockwise from Alaska to southern Asia (30°N), crossing central Asia and moving back to Greenland (Figures 8f and 9c). The Black Sea VGPs are found to be comparable to VGPs from some locations (e.g., Mono Lake) but to be distinct from other locations (e.g., Site ODP-919). A more detailed discussion of this aspect is given in Liu et al. (2019). Based on a $P_i \geq 0.5$ in the Black Sea PSV record, the duration of the short-lived Mono Lake excursion is estimated to be about 0.3 kyr. Between 30 and 40 ka, D-O Events 5–8 can be recognized in Ca/Ti and K/Ti ratios in all Black Sea cores recording the Mono Lake excursion (supporting information Figures S3 and S4). In addition, five AMS ^{14}C ages obtained from Core M72/5-24GC3 provide further constrains for this time interval (Figure 2e). Nevertheless, the estimated duration of the Mono Lake excursion may contain some uncertainties due to its short-lived occurrence and the limited number of samples covering the Mono Lake excursion in the Black Sea PSV record.

During the Mono Lake excursion, the GAD-parallel component derived from the Black Sea PSV record dropped slightly down to 15 μT at about 34.7 ka. This GAD-parallel component of the Mono Lake is fairly strong when compared with the Norwegian-Greenland Sea excursion (7.5 μT) and the Laschamps excursion (−12 μT) in the Black Sea PSV record (Figure 7c). Nevertheless, in the time interval comprising the Laschamps and the Mono Lake excursions, the non-GAD components show fluctuations with amplitudes similar to the rest of the Black Sea record (Figures 7a and 7b). Thus, during the Mono Lake excursion, the variations of GAD-parallel and non-GAD components imply a weakening of the axial dipole field component but persisting nondipole field oscillations at the Black Sea site. Based on the clusters of VGPs from global sites, Negrini et al. (2014) suggested that the Mono Lake excursion is characterized by nonaxial dipole features. Further, the LSMOD.2 model, which covers the Mono Lake excursion, revealed that the axial dipole decreased to a similar strength of the nondipole field (Korte et al., 2019). Although it is not possible to determine the relative strengths of the various field contributions from a single record, similar amplitudes of the GAD-parallel and non-GAD components in the Black Sea PSV record might indicate at least the presence of comparable amounts of axial dipole and nondipole field components during the Mono Lake excursion. To some extent, this is seen in the GGFSS70.1 model (Figure 6d), where the dipole power decays while the nondipole power oscillates about a constant level from about 40 to 16 ka. After the Mono Lake excursion, the Black Sea GAD-parallel component and total field strength, with some fluctuations, show a gradual increase until 14.5 ka.

5. Conclusions

A comprehensive study on 16 sediment cores recovered from the SE Black Sea yielded a high-resolution and high-fidelity record of PSV from 68.9 to 14.5 ka. Normal secular variations, characterized by strong field intensity and normal polarity directions, are represented by a stable dipole field spanning the time intervals from 60.0 to 43.0 ka and from 30.0 to 14.5 ka. The Norwegian-Greenland Sea, the Laschamps, and the Mono Lake excursions, however, are indicated by field intensity lows and an excursional PSV index ($P_i \geq 0.5$) at about 64.5, 41.2, and 34.5 ka, respectively. Based on a PSV index $P_i \geq 0.5$, the duration of the Laschamps excursion is estimated to be ~1.76 kyr, while for the Mono Lake excursion a duration of only ~0.3 kyr was determined.

By converting the Black Sea PSV record into GAD-parallel and non-GAD components, the various field configurations of the three excursion events could be analyzed in some more detail. The Black Sea GAD-parallel component shows coherent variations with the dipole field observed in the Geomagnetic Model GGFSS70.1,

though theoretically comprising also contributions from higher-order multipoles. During the Norwegian-Greenland Sea excursion, the steady decrease of GAD-parallel component was likely related to the decay of the axial dipole field, while the nondipolar field showed oscillation of persisting amplitude. This resulted in fast directional variations at low field intensities but without excursional directions detected. The Laschamps excursion comprises two polarity transitions and a short interval of fully reversed field in between: the N → R and R → N transitions of the Laschamps coincided with the sharp decrease and increase of the axial dipole field, respectively. The reversed polarity phase, evidenced by a negative GAD-parallel component and VGPs at high southern latitudes, was associated with the development of an axial dipole field in opposite direction during the midpoint of the Laschamps excursion. The Mono Lake excursion, characterized by diverging VGP paths from various globally distributed sites, was likely influenced by persisting nondipole field contributions and a reduced axial dipole field contribution, though with higher intensities compared to the Norwegian-Greenland Sea and the Laschamps excursions. In the Black Sea PSV record spanning from 68.9 to 14.5 ka, the non-GAD components related only to nondipole field contributions exhibit fairly stable fluctuations across excursions and normal secular variation intervals, except for relatively weak fluctuations between 67 and 57 ka.

In summary, the Black Sea PSV record, covering field fluctuations from normal secular variations, over excursions, to a short but full reversal, points to a geomagnetic field characterized by a wide dynamic range in intensity and the highly variable superposition of dipole and nondipole contributions from the geodynamo. The three geomagnetic excursions recorded in the Black Sea sediments exhibited field configurations different from each other. However, in order to completely disentangle the complex geodynamo processes inside the Earth's liquid outer core and to further refine the conclusions obtained here, more high-quality studies on sediments from other global locations are needed.

Data Availability Statement

The Black Sea paleomagnetic data discussed in this paper are available in the Pangaea database (paleomagnetic stacks: https://doi.pangaea.de/10.1594/PANGAEA.919401; paleomagnetic results of individual cores: https://doi.pangaea.de/10.1594/PANGAEA.919446; and age models: https://doi.pangaea.de/10.1594/PANGAEA.919427).

Acknowledgments

We thank Steve P. Lund for providing paleomagnetic records of Site ODP-1233, Core PLC08-1, and Core MD98-2181. We thank Jean-Pierre Valet and an anonymous reviewer for their constructive comments and suggestions. We thank S. Plewe, M. Duwe, T. Moldenhawer, and F. Brendel for their technical and logistical help during processing and subsampling of the cores. We also thank the captains and crews of *RV Meteor*, Cruise M72/5, and *RV Maria S. Merian*, Cruise MSM33, for their efforts in providing optimal scientific working conditions. This work was partly funded by the German Research Foundation (Deutsche Forschungsgemeinschaft, DFG SPP 1266 "INTERDYNAMIC" Grants AR 367/9-1 and AR 367/9-2), the Gary Comer Science and Education Foundation, USA, and the Chinese Scholarship Council (CSC Grant 201506180060). Open access funding enabled and organized by Projekt DEAL.

References

Bahr, A., Arz, H. W., Lamy, F., & Wefer, G. (2006). Late glacial to Holocene paleoenvironmental evolution of the Black Sea, reconstructed with stable oxygen isotope records obtained on ostracod shells. *Earth and Planetary Science Letters*, *241*(3–4), 863–875. https://doi.org/10.1016/j.epsl.2005.10.036

Bahr, A., Lamy, F., Arz, H., Kuhlmann, H., & Wefer, G. (2005). Late glacial to Holocene climate and sedimentation history in the NW Black Sea. *Marine Geology*, *214*(4), 309–322. https://doi.org/10.1016/j.margeo.2004.11.013

Biggin, A. J., McCormack, A., & Roberts, A. (2010). Paleointensity database updated and upgraded. *Eos, Transactions American Geophysical Union*, *91*(2), 15. https://doi.org/10.1029/2010eo020003

Bleil, U., & Gard, G. (1989). Chronology and correlation of Quaternary magnetostratigraphy and nannofossil biostratigraphy in Norwegian-Greenland Sea sediments. *Geologische Rundschau*, *78*(3), 1173–1187. https://doi.org/10.1007/BF01829339

Bonhommet, N., & Babkine, J. (1967). Sur la presence d'aimantations iveers es dans la Chaine des Puys. *Comptes Rendus de l'Académie des Sciences*, *264*, 92–94.

Brown, M. C., Donadini, F., Korte, M., Nilsson, A., Korhonen, K., Lodge, A., et al. (2015). GEOMAGIA50.v3: 1. General structure and modifications to the archeological and volcanic database. *Earth, Planets and Space*, *67*(1), 83. https://doi.org/10.1186/s40623-015-0232-0

Brown, M. C., & Korte, M. (2016). A simple model for geomagnetic field excursions and inferences for palaeomagnetic observations. *Physics of the Earth and Planetary Interiors*, *254*, 1–11. https://doi.org/10.1016/j.pepi.2016.03.003

Brown, M. C., Korte, M., Holme, R., Wardinski, I., & Gunnarson, S. (2018). Earth's magnetic field is probably not reversing. *Proceedings of the National Academy of Sciences of the United States of America*, *115*(20), 5111–5116. https://doi.org/10.1073/pnas.1722110115

Cassata, W. S., Singer, B. S., & Cassidy, J. (2008). Laschamp and Mono Lake geomagnetic excursions recorded in New Zealand. *Earth and Planetary Science Letters*, *268*(1–2), 76–88. https://doi.org/10.1016/j.epsl.2008.01.009

Cassidy, J., & Hill, M. J. (2009). Absolute palaeointensity study of the Mono Lake excursion recorded by New Zealand basalts. *Physics of the Earth and Planetary Interiors*, *172*(3–4), 225–234. https://doi.org/10.1016/j.pepi.2008.09.018

Channell, J. E. T. (2006). Late Brunhes polarity excursions (Mono Lake, Laschamp, Iceland Basin and Pringle Falls) recorded at ODP Site 919 (Irminger Basin). *Earth and Planetary Science Letters*, *244*(1–2), 378–393. https://doi.org/10.1016/j.epsl.2006.01.021

Channell, J. E. T., Hodell, D. A., & Curtis, J. H. (2012). ODP Site 1063 (Bermuda Rise) revisited: Oxygen isotopes, excursions and paleointensity in the Brunhes Chron. *Geochemistry, Geophysics, Geosystems*, *13*, Q02001. https://doi.org/10.1029/2011GC003897

Channell, J. E. T., Singer, B. S., & Jicha, B. R. (2020). Timing of Quaternary geomagnetic reversals and excursions in volcanic and sedimentary archives. *Quaternary Science Reviews*, *228*, 106114. https://doi.org/10.1016/j.quascirev.2019.106114

Channell, J. E. T., Vázquez Riveiros, N., Gottschalk, J., Waelbroeck, C., & Skinner, L. C. (2017). Age and duration of Laschamp and Iceland Basin geomagnetic excursions in the South Atlantic Ocean. *Quaternary Science Reviews*, *167*, 1–13. https://doi.org/10.1016/j.quascirev.2017.04.020

Channell, J. E. T., & Xuan, C. (2009). Self-reversal and apparent magnetic excursions in Arctic sediments. *Earth and Planetary Science Letters*, *284*(1–2), 124–131. https://doi.org/10.1016/j.epsl.2009.04.020

Channell, J. E. T., Xuan, C., & Hodell, D. A. (2009). Stacking paleointensity and oxygen isotope data for the last 1.5 Myr (PISO-1500). *Earth and Planetary Science Letters*, *283*(1–4), 14–23. https://doi.org/10.1016/j.epsl.2009.03.012

Chase, Z., McManus, J., Mix, A. C., & Muratli, J. (2014). Southern-ocean and glaciogenic nutrients control diatom export production on the Chile margin. *Quaternary Science Reviews*, *99*, 135–145. https://doi.org/10.1016/j.quascirev.2014.06.015

Coe, R. S., Grommé, S., & Mankinen, E. A. E. A. (1978). Geomagnetic paleointensities from radiocarbon-dated lava flows on Hawaii and the question of the Pacific nondipole low. *Journal of Geophysical Research*, *83*(B4), 1740–1756. https://doi.org/10.1029/jb083ib04p01740

Cullen, V. L., Smith, V. C., & Arz, H. W. (2014). The detailed tephrostratigraphy of a core from the south-east Black Sea spanning the last ~60 ka. *Journal of Quaternary Science*, *29*(7), 675–690. https://doi.org/10.1002/jqs.2739

Dansgaard, W., Johnsen, S. J., Clausen, H. B., Dahl-Jensen, D., Gundestrup, N. S., Hammer, C. U., et al. (1993). Evidence for general instability of past climate from a 250-kyr ice-core record. *Nature*, *364*(6434), 218–220. https://doi.org/10.1038/364218a0

De Vivo, B., Rolandi, G., Gans, P. B., Calvert, A., Bohrson, W. A., Spera, F. J., & Belkin, H. E. (2001). New constraints on the pyroclastic eruptive history of the Campanian volcanic Plain (Italy). *Mineralogy and Petrology*, *73*(1–3), 47–65. https://doi.org/10.1007/s007100170010

Denham, C. R., & Cox, A. (1971). Evidence that the Laschamp polarity event did not occur 13 300–30 400 years ago. *Earth and Planetary Science Letters*, *13*(1), 181–190. https://doi.org/10.1016/0012-821X(71)90122-1

Fabbro, G. N., Druitt, T. H., & Scaillet, S. (2013). Evolution of the crustal magma plumbing system during the build-up to the 22-ka caldera-forming eruption of Santorini (Greece). *Bulletin of Volcanology*, *75*(12), 767. https://doi.org/10.1007/s00445-013-0767-5

Fisher, R. (1953). Dispersion on a sphere. *Proceedings of the Royal Society A: Mathematical, Physical and Engineering Sciences*, *217*(1130), 295–305. https://doi.org/10.1098/rspa.1953.0064

Gillot, P. Y., Labeyrie, J., Laj, C., Valladas, G., Guérin, G., Poupeau, G., & Delibrias, G. (1979). Age of the Laschamp paleomagnetic excursion revisited. *Earth and Planetary Science Letters*, *42*(3), 444–450. https://doi.org/10.1016/0012-821X(79)90053-0

Hoffman, K. A. (1984). Transitional behavior of the geomagnetic field. *Journal of Geomagnetism and Geoelectricity*, *37*(1), 139–146. https://doi.org/10.5636/jgg.37.139

Ingham, E., Turner, G. M., Conway, C. E., Heslop, D., Roberts, A. P., Leonard, G., et al. (2017). Volcanic records of the Laschamp geomagnetic excursion from Mt Ruapehu, New Zealand. *Earth and Planetary Science Letters*, *472*, 131–141. https://doi.org/10.1016/j.epsl.2017.05.023

Kissel, C., Guillou, H., Laj, C., Carracedo, J. C. C., Nomade, S., Perez-Torrado, F., & Wandres, C. (2011). The Mono Lake excursion recorded in phonolitic lavas from Tenerife (Canary Islands): Paleomagnetic analyses and coupled K/Ar and Ar/Ar dating. *Physics of the Earth and Planetary Interiors*, *187*(3–4), 232–244. https://doi.org/10.1016/j.pepi.2011.04.014

Kornprobst, J., & Lénat, J. F. (2019). Changing name for Earth's changing poles. *Eos*, *100*. https://doi.org/10.1029/2019EO117913

Korte, M., Brown, M. C., Panovska, S., & Wardinski, I. (2019). Robust characteristics of the Laschamp and Mono Lake geomagnetic excursions: Results from global field models. *Frontiers in Earth Science*, *7*(April), 1–21. https://doi.org/10.3389/feart.2019.00086

Laj, C., & Channell, J. E. T. (2015). Geomagnetic excursions. In *Treatise on geophysics* (pp. 343–383). Elsevier: Amsterdam. https://doi.org/10.1016/B978-0-444-53802-4.00104-4

Laj, C., Guillou, H., & Kissel, C. (2014). Dynamics of the earth magnetic field in the 10-75 kyr period comprising the Laschamp and Mono Lake excursions: New results from the French Chaîne des Puys in a global perspective. *Earth and Planetary Science Letters*, *387*, 184–197. https://doi.org/10.1016/j.epsl.2013.11.031

Laj, C., & Kissel, C. (2015). An impending geomagnetic transition? Hints from the past. *Frontiers in Earth Science*, *3*(October), 1–10. https://doi.org/10.3389/feart.2015.00061

Laj, C., Kissel, C., & Beer, J. (2004). High resolution global paleointensity stack since 75 kyr (GLOPIS-75) calibrated to absolute values. *Geophysical Monograph Series*, *145*, 255–265. https://doi.org/10.1029/145GM19

Laj, C., Kissel, C., Mazaud, A., Channell, J. E. T., & Beer, J. (2000). North Atlantic palaeointensity stack since 75 ka (NAPIS-75) and the duration of the Laschamp event. *Philosophical Transactions of the Royal Society A: Mathematical, Physical and Engineering Sciences*, *358*(1768), 1009–1025. https://doi.org/10.1098/rsta.2000.0571

Laj, C., Kissel, C., & Roberts, A. P. (2006). Geomagnetic field behavior during the Iceland Basin and Laschamp geomagnetic excursions: A simple transitional field geometry? *Geochemistry, Geophysics, Geosystems*, *7*, Q03004. https://doi.org/10.1029/2005GC001122

Lamy, F., Arz, H. W., Bond, G. C., Bahr, A., & Pätzold, J. (2006). Multicentennial-scale hydrological changes in the Black Sea and northern Red Sea during the Holocene and the Arctic/North Atlantic oscillation. *Paleoceanography*, *21*, PA1008. https://doi.org/10.1029/2005PA001184

Leonhardt, R., Fabian, K., Winklhofer, M., Ferk, A., Laj, C., & Kissel, C. (2009). Geomagnetic field evolution during the Laschamp excursion. *Earth and Planetary Science Letters*, *278*(1–2), 87–95. https://doi.org/10.1016/j.epsl.2008.11.028

Liddicoat, J. C., & Coe, R. S. (1979). Mono Lake geomagnetic excursion. *Journal of Geophysical Research*, *84*, 261–271. https://doi.org/10.1029/JB084iB01p00261

Liu, J., Nowaczyk, N. R., Frank, U., & Arz, H. (2019). Geomagnetic paleosecular variation record spanning from 40 to 20 ka—Implications for the Mono Lake excursion from Black Sea sediments. *Earth and Planetary Science Letters*, *509*, 114–124. https://doi.org/10.1016/j.epsl.2018.12.029

Liu, J., Nowaczyk, N. R., Frank, U., & Arz, H. W. (2018). A 20–15 ka high-resolution paleomagnetic secular variation record from Black Sea sediments—No evidence for the 'Hilina Pali excursion'? *Earth and Planetary Science Letters*, *492*, 174–185. https://doi.org/10.1016/j.epsl.2018.04.014

Lougheed, B. C., & Obrochta, S. P. (2019). A rapid, deterministic age-depth modeling routine for geological sequences with inherent depth uncertainty. *Paleoceanography and Paleoclimatology*, *34*, 122–133. https://doi.org/10.1029/2018PA003457

Løvlie, R. (1989). Palaeomagnetic excursions during the last interglacial/glacial cycle: A synthesis. *Quaternary International*, *3–4*, 5–11. https://doi.org/10.1016/1040-6182(89)90068-2

Lund, S. P. (2018). A new view of long-term geomagnetic field secular variation. *Frontiers in Earth Science*, *6*(May), 1–13. https://doi.org/10.3389/feart.2018.00040

Lund, S. P., Benson, L., Negrini, R. M., Liddicoat, J., & Mensing, S. (2017). A full-vector paleomagnetic secular variation record (PSV) from Pyramid Lake (Nevada) from 47–17ka: Evidence for the successive Mono Lake and Laschamp Excursions. *Earth and Planetary Science Letters*, *458*, 120–129. https://doi.org/10.1016/j.epsl.2016.09.036

Lund, S. P., Liddicoat, J. C., Lajoie, K. R., Henyey, T. L., & Robinson, S. W. (1988). Paleomagnetic evidence for long-term (10^4 year) memory and periodic behavior in the Earth's core dynamo process. *Geophysical Research Letters*, *15*(10), 1101–1104. https://doi.org/10.1029/GL015i010p01101

Lund, S. P., Schwartz, M., Keigwin, L., & Johnson, T. (2005). Deep-sea sediment records of the Laschamp geomagnetic field excursion (~41,000 calendar years before present). *Journal of Geophysical Research*, *110*, B04101. https://doi.org/10.1029/2003JB002943

Lund, S. P., Schwartz, M., & Stott, L. (2017). Long-term palaeomagnetic secular variation and excursions from the western equatorial Pacific Ocean (MIS2-4). *Geophysical Journal International*, *209*, 587–596. https://doi.org/10.1093/gji/ggx029

Lund, S. P., Stoner, J., Channell, J., & Lamy, F. (2007). Detailed paleomagnetic and rock magnetic variability within three high-resolution study intervals from Site 1233. In *Proceedings of the Ocean Drilling Program, 202 Scientific Results*, *202*(March 2005). https://doi.org/10.2973/odp.proc.sr.202.212.2007

Lund, S. P., Stoner, J., & Lamy, F. (2006). Late Quaternary paleomagnetic secular variation and chronostratigraphy from ODP sites 1233 and 1234. In *Proceedings of the Ocean Drilling Program: Scientific Results*, *202*(February). https://doi.org/10.2973/odp.proc.sr.202.208.2006

Lund, S. P., Stoner, J. S., Channell, J. E. T., & Acton, G. (2006). A summary of Brunhes paleomagnetic field variability recorded in ocean drilling program cores. *Physics of the Earth and Planetary Interiors*, *156*(3–4), 194–204. https://doi.org/10.1016/j.pepi.2005.10.009

Lund, S. P., Williams, T., Acton, G. D., Clement, B., & Okada, M. (2001). Brunhes chron magnetic field excursions recovered from Leg 172. In *Proceedings of the Ocean Drilling Program, Scientific Results*, *172*(February). https://doi.org/10.2973/odp.proc.sr.172.216.2001

Mazaud, A., Sicre, M. A., Ezat, U., Pichon, J. J., Duprat, J., Laj, C., et al. (2002). Geomagnetic-assisted stratigraphy and sea surface temperature changes in core MD94-103 (southern Indian Ocean): Possible implications for north-south climatic relationships around H4. *Earth and Planetary Science Letters*, *201*(1), 159–170. https://doi.org/10.1016/S0012-821X(02)00662-3

Ménabréaz, L., Thouveny, N., Bourlès, D. L., Deschamps, P., Hamelin, B., & Demory, F. (2011). The Laschamp geomagnetic dipole low expressed as a cosmogenic ^{10}Be atmospheric overproduction at ~41 ka. *Earth and Planetary Science Letters*, *312*(3–4), 305–317. https://doi.org/10.1016/j.epsl.2011.10.037

Merrill, R. T., & McFadden, P. L. (1999). Geomagnetic polarity transitions. *Reviews of Geophysics*, *37*(2), 201–226. https://doi.org/10.1029/1998RG900004

Negrini, R. M., McCuan, D. T., Horton, R. A., Lopez, J. D., Cassata, W. S., Channell, J. E. T., et al. (2014). Nongeocentric axial dipole field behavior during the Mono Lake excursion. *Journal of Geophysical Research: Solid Earth*, *119*, 2567–2581. https://doi.org/10.1002/2013JB010846

Nowaczyk, N. R., Antonow, M., Knies, J., & Spielhagen, R. F. (2003). Further rock magnetic and chronostratigraphic results on reversal excursions during the last 50 ka as derived from northern high latitudes and discrepancies in precise AMS 14C dating. *Geophysical Journal International*, *155*(3), 1065–1080. https://doi.org/10.1111/j.1365-246X.2003.02115.x

Nowaczyk, N. R., Arz, H. W. W., Frank, U., Kind, J., & Plessen, B. (2012). Dynamics of the Laschamp geomagnetic excursion from Black Sea sediments. *Earth and Planetary Science Letters*, *351-352*, 54–69. https://doi.org/10.1016/j.epsl.2012.06.050

Nowaczyk, N. R., & Baumann, M. (1992). Combined high-resolution magnetostratigraphy and nannofossil biostratigraphy for late Quaternary Arctic Ocean sediments. *Deep Sea Research Part A. Oceanographic Research Papers*, *39*(2), S567–S601. https://doi.org/10.1016/S0198-0149(06)80021-X

Nowaczyk, N. R., Frank, U., Kind, J., & Arz, H. W. (2013). A high-resolution paleointensity stack of the past 14 to 68 ka from black sea sediments. *Earth and Planetary Science Letters*, *384*, 1–16. https://doi.org/10.1016/j.epsl.2013.09.028

Nowaczyk, N. R., & Frederichs, T. W. (1999). Geomagnetic events and relative palaeointensity variations during the past 300 ka as recorded in Kolbeinsey Ridge sediments, Iceland Sea: Indication for a strongly variable geomagnetic field. *International Journal of Earth Sciences*, *88*(1), 116–131. https://doi.org/10.1007/s005310050250

Nowaczyk, N. R., Jiabo, L., Frank, U., & Arz, H. W. (2018). A high-resolution paleosecular variation record from Black Sea sediments indicating fast directional changes associated with low field intensities during marine isotope stage (MIS) 4. *Earth and Planetary Science Letters*, *484*, 15–29. https://doi.org/10.1016/j.epsl.2017.12.009

Nowaczyk, N. R., & Knies, J. (2000). Magnetostratigraphic results from the eastern Arctic Ocean: AMS ^{14}C ages and relative palaeointensity data of the Mono Lake and Laschamp geomagnetic reversal excursions. *Geophysical Journal International*, *140*(1), 185–197. https://doi.org/10.1046/j.1365-246X.2000.00001.x

Panovska, S., & Constable, C. G. (2017). An activity index for geomagnetic paleosecular variation, excursions, and reversals. *Geochemistry, Geophysics, Geosystems*, *18*, 1366–1375. https://doi.org/10.1002/2016GC006668

Panovska, S., Constable, C. G., & Brown, M. C. (2018). Global and regional assessments of paleosecular variation activity over the past 100 ka. *Geochemistry, Geophysics, Geosystems*, *19*(5), 1559–1580. https://doi.org/10.1029/2017GC007271

Panovska, S., Constable, C. G., & Korte, M. (2018). Extending global continuous geomagnetic field reconstructions on timescales beyond human civilization. *Geochemistry, Geophysics, Geosystems*, *19*, 4757–4772. https://doi.org/10.1029/2018GC007966

Philippe, É. G. H., Valet, J. P., St-Onge, G., & Thevarasan, A. (2018). Are paleomagnetic records from U-channels appropriate for studies of reversals and excursions? *Geochemistry, Geophysics, Geosystems*, *19*, 4130–4142. https://doi.org/10.1029/2018GC007803

Plenier, G., Valet, J. P., Guérin, G., Lefèvre, J.-C., LeGoff, M., & Carter-Stiglitz, B. (2007). Origin and age of the directions recorded during the Laschamp event in the Chaîne des Puys (France). *Earth and Planetary Science Letters*, *259*(3–4), 414–431. https://doi.org/10.1016/j.epsl.2007.04.039

Roberts, A. P. (2008). Geomagnetic excursions: Knowns and unknowns. *Geophysical Research Letters*, *35*, L17307. https://doi.org/10.1029/2008GL034719

Roberts, A. P., & Winklhofer, M. (2004). Why are geomagnetic excursions not always recorded in sediments? Constraints from post-depositional remanent magnetization lock-in modelling. *Earth and Planetary Science Letters*, *227*(3–4), 345–359. https://doi.org/10.1016/j.epsl.2004.07.040

Shumilovskikh, L. S., Marret, F., Fleitmann, D., Arz, H. W., Nowaczyk, N. R., & Behling, H. (2013). Eemian and Holocene sea-surface conditions in the southern Black Sea: Organic-walled dinoflagellate cyst record from core 22-GC3. *Marine Micropaleontology*, *101*, 146–160. https://doi.org/10.1016/j.marmicro.2013.02.001

Sicre, M., Labeyrie, L., Ezat, U., Duprat, J., Turon, J., Schmidt, S., et al. (2005). Mid-latitude Southern Indian Ocean response to Northern Hemisphere Heinrich events. *Earth and Planetary Science Letters*, *240*(3–4), 724–731. https://doi.org/10.1016/j.epsl.2005.09.032

Simon, Q., St-Onge, G., & Hillaire-Marcel, C. (2012). Late Quaternary chronostratigraphic framework of deep Baffin Bay glaciomarine sediments from high-resolution paleomagnetic data. *Geochemistry, Geophysics, Geosystems*, *13*, Q0AO03. https://doi.org/10.1029/2012GC004272

Singer, B. S., Jicha, B. R., He, H., & Zhu, R. (2014). Geomagnetic field excursion recorded 17 ka at Tianchi Volcano, China: New $^{40}Ar/^{39}Ar$ age and significance. *Geophysical Research Letters*, *41*, 2794–2802. https://doi.org/10.1002/2014GL059439

Soulet, G., Ménot, G., Bayon, G., Rostek, F., Ponzevera, E., Toucanne, S., et al. (2013). Abrupt drainage cycles of the Fennoscandian Ice Sheet. *Proceedings of the National Academy of Sciences*, *110*(17), 6682–6687. https://doi.org/10.1073/pnas.1214676110

Svensson, A., Andersen, K. K., Bigler, M., Clausen, H. B., Dahl-Jensen, D., Davies, S. M., et al. (2008). A 60 000 year Greenland stratigraphic ice core chronology. *Climate of the Past, European Geosciences Union*, *4*(1), 47–57. https://doi.org/10.5194/cp-4-47-2008

Thouveny, N., Carcaillet, J., Moreno, E., Leduc, G., & Nérini, D. (2004). Geomagnetic moment variation and paleomagnetic excursions since 400 kyr BP: A stacked record from sedimentary sequences of the Portuguese margin. *Earth and Planetary Science Letters*, *219*(3–4), 377–396. https://doi.org/10.1016/S0012-821X(03)00701-5

Valet, J. P., Meynadier, L., & Guyodo, Y. (2005). Geomagnetic dipole strength and reversal rate over the past two million years. *Nature*, *435*(7043), 802–805. https://doi.org/10.1038/nature03674

Valet, J. P., Meynadier, L., Simon, Q., & Thouveny, N. (2016). When and why sediments fail to record the geomagnetic field during polarity reversals. *Earth and Planetary Science Letters*, *453*, 96–107. https://doi.org/10.1016/j.epsl.2016.07.055

Valet, J. P., & Plenier, G. (2008). Simulations of a time-varying non-dipole field during geomagnetic reversals and excursions. *Physics of the Earth and Planetary Interiors*, *169*(1–4), 178–193. https://doi.org/10.1016/j.pepi.2008.07.031

Valet, J. P., Plenier, G., & Herrero-Bervera, E. (2008). Geomagnetic excursions reflect an aborted polarity state. *Earth and Planetary Science Letters*, *274*(3–4), 472–478. https://doi.org/10.1016/j.epsl.2008.07.056

Wegwerth, A., Dellwig, O., Kaiser, J. Ô., Ménot, G., Bard, E., Shumilovskikh, L., et al. (2014). Meltwater events and the Mediterranean reconnection at the Saalian-Eemian transition in the Black Sea. *Earth and Planetary Science Letters*, *404*, 124–135. https://doi.org/10.1016/j.epsl.2014.07.030

Wegwerth, A., Dellwig, O., Wulf, S., Plessen, B., Kleinhanns, I. C., Nowaczyk, N. R., et al. (2019). Major hydrological shifts in the Black Sea "Lake" in response to ice sheet collapses during MIS 6 (130–184 ka BP). *Quaternary Science Reviews*, *219*, 126–144. https://doi.org/10.1016/j.quascirev.2019.07.008

Wicht, J., & Meduri, D. G. (2016). A Gaussian model for simulated geomagnetic field reversals. *Physics of the Earth and Planetary Interiors*, *259*, 45–60. https://doi.org/10.1016/j.pepi.2016.07.007

Wiers, S., Snowball, I. F., O'Regan, M., & Almqvist, B. (2019). Late Pleistocene chronology of sediments from the Yermak Plateau and uncertainty in dating based on geomagnetic excursions. *Geochemistry, Geophysics, Geosystems*, *20*, 2018GC007920. https://doi.org/10.1029/2018GC007920

Xuan, C., & Channell, J. E. T. (2010). Origin of apparent magnetic excursions in deep-sea sediments from Mendeleev-Alpha Ridge, Arctic Ocean. *Geochemistry, Geophysics, Geosystems*, *11*, Q02003. https://doi.org/10.1029/2009GC002879

Xuan, C., Channell, J. E. T., Polyak, L., & Darby, D. A. (2012). Paleomagnetism of Quaternary sediments from Lomonosov Ridge and Yermak Plateau: Implications for age models in the Arctic Ocean. *Quaternary Science Reviews*, *32*, 48–63. https://doi.org/10.1016/j.quascirev.2011.11.015

References From the Supporting Information

Croudace, I. W., Rindby, A., & Rothwell, R. G. (2006). ITRAX: Description and evaluation of a new multi-function X-ray core scanner. *Geological Society, London, Special Publications*, *267*(1), 51–63. https://doi.org/10.1144/GSL.SP.2006.267.01.04

Kirschvink, J. L. (1980). The least-squares line and plane and the analysis of palaeomagnetic data. *Geophysical Journal International*, *62*(3), 699–718. https://doi.org/10.1111/j.1365-246X.1980.tb02601.x

Kwiecien, O., Arz, H. W., Lamy, F., Wulf, S., Bahr, A., Röhl, U., & Haug, G. H. (2008). Estimated reservoir ages of the black sea since the last glacial. *Radiocarbon*, *50*(1), 99–118. https://doi.org/10.1017/S0033822200043393

Major, C. O., Goldstein, S. L., Ryan, W. B. F. F., Lericolais, G., Piotrowski, A. M., & Hajdas, I. (2006). The co-evolution of Black Sea level and composition through the last deglaciation and its paleoclimatic significance. *Quaternary Science Reviews*, *25*(17–18), 2031–2047. https://doi.org/10.1016/j.quascirev.2006.01.032

Röhl, U., & Abrams, L. J. (2000). High-resolution, downhole, and nondestructive core measurements from Sites 999 and 1001 in the Caribbean Sea: Application to the Late Paleocene thermal maximum. *Procedings of the Ocean Drilling Program, Scientific Results*, *165*, 191–203. https://doi.org/10.2973/odp.proc.sr.165.009.2000

Shumilovskikh, L. S., Tarasov, P., Arz, H. W., Fleitmann, D., Marret, F., Nowaczyk, N. R., et al. (2012). Vegetation and environmental dynamics in the southern Black Sea region since 18kyr BP derived from the marine core 22-GC3. *Palaeogeography, Palaeoclimatology, Palaeoecology*, *337-338*, 177–193. https://doi.org/10.1016/j.palaeo.2012.04.015